Ann. Geophys. Discuss., https://doi.org/10.5194/angeo-2019-46
Manuscript under review for journal Ann. Geophys.
Discussion started: 7 May 2019

Annales Geophysicae Discussions
Open Access
EGU

Model of Propagation of VLF Beams in the Waveguide Earth-Ionosphere. Principles of Tensor Impedance Method in Multilayered Gyrotropic Waveguides.

Yuriy Rapoport[#1], Vladimir Grimalsky[*2], Victor Fedun[~3], Oleksiy Agapitov [⊥4], John Bonnell[⊥5], Asen Grytsai[#6], Gennadi Milinevsky[#ε7], Alex Liashchuk[±8], Alexander Rozhnoi[ϕ9], Maria Solovieva[ϕ10], Andrey Gulin[#11]

[#]Taras Shevchenko National University of Kyiv, Ukraine
[*]Autonomous University of State Morelos (UAEM), Mexico
[~]The University of Sheffield, UK
[⊥]University of California, Berkeley, USA
[ε] College of Physics, International Center of Future Science, Jilin University, Changchun, China
[±]National Center for Control and Testing of Space Facilities of the State Agency of Ukraine
[ϕ]Institute of the Earth Physics, RAS, Moscow, Russia

[1]yuriy.rapoport@gmail.com, [2]v_grim@yahoo.com, [3]v.fedun@sheffield.ac.uk, [4]oleksiy.agapitov@gmail.com, [5]jwbonnell@berkeley.edu, [6]a.grytsai@gmail.com, [7]genmilinevsky@gmail.com, [8]alex.liashchukk@gmail.com, [9]rozhnoi@ifz.ru, [10]MCSolovieva@gmail.com, [11]mytimetosay@gmail.com

Correspondence to: Yuriy Rapoport (yuriy.rapoport@gmail.com)

Abstract. Modeling propagation of VLF electromagnetic beams in the waveguide earth-ionosphere (WGEI) is of a great importance because variation in the characteristics of these waves is an effective instrument for diagnostics the influences on the ionosphere "from above" (Sun-Solar Wind-Magnetosphere-Ionosphere), "from below" (the most powerful meteorological, seismogenic and other sources in the lower atmosphere and lithosphere/Earth, such as hurricanes, earthquakes, tsunamis etc.), from inside the ionosphere (strong thunderstorms and lightning discharges) and even from the far space (such as gamma-flashes, cosmic rays etc.). Thus, VLF became one of the most universal instrument for monitoring the Space Weather in the direct sense of this term, i.e. the state of the Sun-Earth space and the ionosphere as it is particularly determined by all possible relatively powerful sources, wherever they are placed. This paper is devoted mostly to modelling VLF electromagnetic beam propagation in the WGEI. We present a new tensor impedance method for modelling propagation of electromagnetic beams (TIMEB) in a multi-layered/inhomogeneous waveguide. Suppose that such a waveguide, i.e. WGEI, possesses the gyrotropy and inhomogeneity with a thick cover layer placed above the waveguide. Note a very useful and attractive feature of the proposed TIMEB method: in spite of a large thickness of the waveguide cover layer, the proposed effective impedance approach reflects an impact of such a cover on the electromagnetic (EM) waves, which propagate in the waveguide. This impedance approach can be applied for EM waves/beams in layered gyrotropic/anisotropic active media in very wide frequency range, from VLF to optics. Moreover, this approach can be applied to calculations of EM waves/beams propagation in the media of an artificial origin such as metamaterial microwave

or optical waveguides. The results of the modelling the propagation of VLF beams in the WGEI are included. The qualitative comparison between the theory and experimental observation of increasing losses of VLF waves in the WGEI is discussed. The new proposed method and its further development allows the comparison with the results of the future rocket experiment. This method allows to model (i) excitation of the VLF modes in the WGEI and their excitation by the typical VLF sources, such as radio wave transmitters and lightning discharges and (ii) leakage of VLF waves/beams into the upper ionosphere/magnetosphere.

***Keywords* — ionosphere, atmosphere, VLF, tensor impedance, gyrotropy, layered waveguide, beam, electromagnetic wave, boundary conditions, ionospheric disturbances, vertical coupling processes**

1 Introduction

This paper is dedicated to the propagation in the system Lithosphere–Atmosphere–Ionosphere–Magnetosphere (LAIM) of electromagnetic (EM) waves /beams in the radio range, with particular applications to very low frequencies (VLF). This topic became very actual due to the following reasons. (1) Variation in the characteristics of these waves is now an effective instrument for the diagnostics of "ionospheric weather" as a part of the Space Weather (Hapgood 2017; Yigit et al. 2016; Richmond 1996) in its direct meaning: the state of the Sun-Earth space and the ionosphere in particular determined by all possible sufficiently powerful sources, wherever they are placed. Change in the characteristics (amplitude and phase) of the VLF waves propagating in the waveguide earth-ionosphere (WGEI) reflects the corresponding variations in the ionospheric electrodynamics characteristics (complex dielectric permittivity) and respectively, the influences on the ionosphere "from above" (Sun-Solar Wind-Magnetosphere Ionosphere (WINDMII) (Patra et al., 2011; Koskinen, 2011; Boudjada et al., 2012; Wu et al., 2016), "from below" (the most powerful meteorological, seismogenic and other sources in the lower atmosphere and lithosphere/Earth, such as cyclones and hurricanes (Nina et al., 2017; Rozhnoi et al., 2014; Chou et al., 2015), earthquakes (Hayakawa, 2015; Surkov and Hayakawa, 2014; Sanchez-Dulcet et al., 2015), tsunamis etc. or from inside the ionosphere (strong thunderstorms and lightning discharges, terrestrial gamma-ray flashes or sprite streamers (Cummer et al., 1998; Qin et al., 2012; Dwyer 2012; Dwyer and Uman, 2014; Cummer et al., 2014; Mezentsev et al., 2018). Note that the VLF signals are very important for the merging of the atmospheric physics and space plasma physics with the astrophysics and high energy physics. The corresponding "intersection area" for these two disciplines includes cosmic rays and very popular now objects of investigation – high-altitude discharges (sprites), anomalous X-ray bursts, powerful gamma-ray bursts etc. The key phenomena for the occurrence of all of these objects are runaway electrons with runaway breakdown, and one of the necessary conditions of them is the presence of cosmic rays, consequently these phenomena are intensified during the air showers generating by cosmic particles (Gurevich and Zubin 2001; Gurevich et al. 2009).. The runaway breakdown and lightning discharges including high-latitude ones case radio emission both in HF range, which could be observed using LOFAR and other radio telescopes (Buitink et al., 2014; Scholten et al., 2017; Hare 2018), and in the VLF range. Corresponding experimental research include measurements of the VLF characteristics by the international measurement system of the pairs "transmitted-receiver" separated by a distance of a couple of thousand km (Biagi et al.,

2011; Biagi et al., 2015). Another international system is based on the measurements of VLF characteristics for the characterization of the thunderstorms with the lightning discharges/World Wide Lightning Location Network (WWLLN) (Lu et al. 2019). (2) Intensification of the magnetospheric research, wave processes, particle distribution and wave-particle interaction in the magnetosphere including radiation belts leads to the great interest to the VLF plasma waves, in particular whistlers (Artemyev et al., 2013; Agapitov et al., 2014; Agapitov et al., 2018).

The differences of our proposed model from the known ones used for the simulation of the VLF waves in the WGEI are the following. (1) In distinction to the impedance invariant imbedding model (Shalashov and Gospodchikov, 2010; Kim and Kim, 2016), our model provides optimal, for definite class of problems, which we consider, balance between the analytical and numerical approaches and is, in fact combined analytical-numerical one, basing on matrix sweep, method (Samarskii, 2001). As a result, this model allows to obtain analytically the tensor impedance and at the same time, provides high effectiveness and stability of the modelling. (2) In distinction to the full-wave finite difference time domain (FDTD) models such as (Chevalier and Inan, 2006; Marshall et al., 2017; Yaxin et al., 2012; Azadifar et al., 2017), our method provides very physically clear lower and upper boundary conditions, in particular physically justified upper boundary conditions corresponding to the radiation of the waves propagation in the WGEI to the upper ionosphere/magnetosphere. This allows in a perspective to determine the leakage modes and to interpret not only ground-based, but also satellite measurements of the VLF beam characteristics. (3) In distinction to the models (Kuzichev and Shklyar, 2010; Kuzichev et al., 2018; Lehtinen and Inan, 2009; Lehtinen and Inan, 2008) based on the mode presentations and made in the frequency domain, we use the combined approach, This approach includes condition of the radiation at the altitudes of the F region, equivalent impedance conditions in the lower E region and at the lower boundary of the WGEI, mode approach, and finally, beam method. This combined approach, finally, creates the possibility to interpret adequately data of both ground and satellite detection on the EM wave/beam propagating in the WGEI and these which leakage from the WGEI into the upper ionosphere/magnetosphere. Some other details on the distinctions from the previously published models are given below in Sect. 3.

The methods of effective boundary conditions, in particular effective impedance conditions (Tretyakov, 2003; Senior and Volakis, 1995; Kurushin and Nefedov, 1983) are well-known and can be used, in particular, for the layered metal-dielectric, metamaterial and gyrotropic active layered and waveguiding media of different types (Tretyakov, 2003; Senior and Volakis, 1995; Kurushin and Nefedov, 1983; Collin, 2001; Weit, 1996) including plasma-like solid state (Ruibys and Tolutis, 1983) and space plasma (Weit, 1996) media. The plasma wave processes in the waveguide structures metal-semiconductor-dielectric, placed into the external magnetic field, were widely investigated (Ruibys and Tolutis, 1983; Maier, 2007; Tarkhanyan and Uzunoglu, 2006) in various frequency ranges, from radio to optical ones. Corresponding waves are applied in modern plasmonics and in non-destructive testing of semiconductor interfaces. It is of interest to realize the resonant interactions of volume and surface electromagnetic waves in these structures, so the simulations of the wave spectrum there are important. To describe such complex layered structures, it is very convenient and effective to use impedance approach (Tretyakov, 2003; Senior and Volakis, 1995; Kurushin and Nefedov, 1983). As a rule, impedance

boundary conditions are used, when the layer covering waveguide is thin (Senior and Volakis, 1995; Kurushin and Nefedov, 1983). One of the known exclusions is the impedance invariant imbedding model, the distinction to which of our new method has been mentioned above. Our new approach TIMEB, proposed in the present paper has the set of very attractive, for practical purposes, features. These features are: (i) the surface impedance characterizes cover layer of finite thickness, and this impedance is expressed analytically; (ii) the method allows an effective modelling of 3D beam propagating in the gyrotropic waveguiding structure; (iii) finally, if the considered waveguide can be modified by any external influence such as bias magnetic or electric fields, or by any extra wave or energy beams (such as acoustic or quasistatic fields etc.), the corresponding modification of the characteristics (phase and amplitude) of the electromagnetic VLF beam propagating in the waveguide structure can be modelled.

Our approach was targeting properly and is suitable for the farther important development which will allow to solve also the following problems, which continue the list presented above: (iv) the problem of the excitation of the waveguide by the waves incident on the considered structure from above could be solved as well with the slight modification of the presented model, with inclusion also ingoing waves; (v) consider a plasma-like system placed into the external magnetic field, such as the LAIM system (Grimalsky et al., 1999 a, b) or dielectric-magnetized semiconductor structure; then the waves radiated outside the waveguiding structure (such as helicons (Ruibys and Tolutis, 1983) or whistlers (Weit, 1996)) and the waveguide modes could be considered altogether; (vi) adequate boundary radiation conditions on the upper boundary of the covering layer are derived; and, based on this (and absence of ingoing waves), the leakage modes above the upper boundary of the structure (in other words, upper boundary of covering layer), will be searched with the farther development of the model, delivered in the present paper. Namely, the process of the leakage of the electromagnetic waves from the (opened) waveguide, then their transformation into magnetized plasma waves, propagating along magnetic field lines, and, possibly, excitation of the waveguiding modes by the waves incident on the system from external space (Walker, 1976), can be modelled as a whole. Such a modification can be measured, characterising the external fields and corresponding field sources, caused the above mentioned waveguide modification. Combining with the proper measurements of the phases and amplitudes of the electromagnetic waves, propagating in the waveguiding structures and leakage waves, the model possessing the above mentioned features can be used for searching, and even monitoring the external influences on the layered gyrotropic active artificial or natural media, for example microwave or optical waveguides or the system LAIM and WGEI, respectively.

The structure of the paper is as follows. In Sect. 2 formulation of the problem is presented. In Sect. 3 the algorithm is presented, including the determination of the conditions of radiation of the VLF waves/beams into the upper ionosphere/magnetosphere at the upper boundary, placed in the F region at the altitude (250-400) km; effective tensor impedance boundary conditions at the upper boundary (~ 85 km) of the effective WGEI; and finally the 3D model of the propagation of the VLF beam in the WGEI, which we call TIMEB, because in fact the beam method is combined with tensor impedance method. The questions on the mode presentation and leakage modes of VLF are discussed very briefly, because the corresponding details will be presented in the next papers. In Sect. 4, the results of numerical modelling are presented. In

Ann. Geophys. Discuss., https://doi.org/10.5194/angeo-2019-46
Manuscript under review for journal Ann. Geophys.
Discussion started: 7 May 2019

Sect. 5, the discussion is presented, including an example of the qualitative comparison between the results of our theory and an experiment; and the future rocket experiment on the measurements of the characteristics of VLF signal, radiated from the VLF transmitter and propagating in the WGEI and penetrating into the upper ionosphere. Finally, conclusions are presented.

2 Formulation of the problem

The VLF electromagnetic (EM) waves with frequencies f = 10 - 100 kHz can propagate along the Earth's surface for long distances >1000 km. The Earth's surface of a high conductivity z = 0 and the ionosphere F-layer z = 300 km form the VLF waveguide, see Fig. 1. The propagation of the VLF electromagnetic radiation excited by a near-Earth antenna within the WGEI should be described by the full set of the Maxwell equations in the isotropic atmosphere $0 < z < 60$ km, the approximately isotropic ionosphere D-layer 60 km $< z <$ 75 km, and the anisotropic E- and F- layers of the ionosphere, due to the geomagnetic field $\bar{H}_0$, added by the boundary conditions at the Earth's surface and at the F-layer.

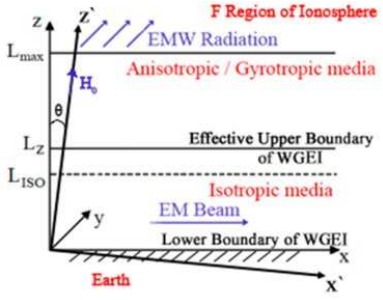

Figure 1. The geometry of the anisotropic/gyrotropic waveguide. EM waves propagate in OX direction. $\bar{H}_0$ is the external magnetic field. The (effective) WGEI for EM waves occupies the region $0 < z < L_z$. Isotropic media occupies the region $0 < z < L_{ISO}$, $L_{ISO} < L_z$. Anisotropic/gyrotropic media occupies the region $L_{ISO} < z < L_{max}$. Covering layer occupies the region $L_z < z < L_{max}$. WG includes isotropic region $0 < z < L_{ISO}$ and a part of anisotropic region $L_z < z < L_{max}$. It is supposed that the anisotropic region is relatively small part of the WG, $(L_z - L_{ISO})/L_z \sim$ (0.1-0.2). At the upper boundary of covering layer ($z = L_{max}$) the radiation of EM to the external region ($z > L_{max}$) is accounted for with the proper boundary conditions. Integration of the equations describing the EM field propagation allows to obtain effective impedance boundary conditions at the upper boundary of effective WG ($z = L_z$). These boundary conditions effectively includes all the effect on the wave propagation of the covering layer and the radiation (at $z = L_{max}$) to the external region ($z > L_{max}$). θ is the angle between the directions of the vertical axis z and geomagnetic field $\bar{H}_0$. The coordinate system $x'y'z'$ is connected with the geomagnetic field: $\bar{H}_0$ is directed along z' axis, lies in the plane xz, and the planes $x'z'$ and xz coincide with each other.

3. Algorithm

We present here the algorithm of the new proposed method, staying in details only on the main subject of the present paper, in particular on the boundary conditions, impedance method and the method for the beam propagation in the WGEI. The

Ann. Geophys. Discuss., https://doi.org/10.5194/angeo-2019-46
Manuscript under review for journal Ann. Geophys.
Discussion started: 7 May 2019

other parts of the method, connected with the mode presentation of the excitation of WGEI by a given current source and the reflection of the EM waves from the effective upper boundary of the WGEI and leakage of the EM waves from the WGEI to the upper ionosphere/magnetosphere, will be outlined here only very briefly and will become the subjects of the next papers.

3.1 Direct and inverse tensors characterizing the ionosphere

In the next subsections we will derive the formulas describing the transfer of the boundary conditions at the upper boundary ($z=L_{max}$), Fig. 1, resulting in the tensor impedance conditions at the upper boundary of the effective WGEI ($z=L_i$). To make this, we need, firstly, to describe the tensors, characterizing the ionosphere. The monochromatic EM field is considered with the components of EM field ~ $\exp(i\omega t)$. The main goal is to transfer the EM boundary conditions from the upper ionosphere at the height $L_z \sim 250 - 400$ km to the lower ionosphere $L_z \sim 70 - 90$ km. The vertical axis is OZ, the inclination angle of the geomagnetic field is Θ_I (Fig. 1). The anisotropic medium is inhomogeneous along OZ axis only and is characterized by the tensor permittivity $\hat{\varepsilon}(\omega,z)$ or by the inverse tensor $\hat{\beta}(\omega,z)=\hat{\varepsilon}^{-1}(\omega,z)$: $\vec{E}=\hat{\beta}(\omega,z)\cdot\vec{D}$, where $\vec{D}$ is the electric induction. Below the absolute units are utilized. The expressions for the components of the effective permittivity of the ionosphere are in the coordinate frame $X'YZ'$ where OZ' axis is aligned along the geomagnetic field $\vec{H}_0$:

$$\hat{\varepsilon}' = \begin{pmatrix} \varepsilon_1 & \varepsilon_h & 0 \\ -\varepsilon_h & \varepsilon_1 & 0 \\ 0 & 0 & \varepsilon_3 \end{pmatrix}, \quad \varepsilon_1 = 1 - \frac{\omega_{pe}^2\cdot(\omega - i\nu_e)}{((\omega - i\nu_e)^2 - \omega_{He}^2)\cdot\omega} - \frac{\omega_{pi}^2\cdot(\omega - i\nu_i)}{((\omega - i\nu_i)^2 - \omega_{Hi}^2)\cdot\omega}, \; \varepsilon_h \equiv ig;$$
$$g = -\frac{\omega_{pe}^2\cdot\omega_{He}}{((\omega - i\nu_e)^2 - \omega_{He}^2)\cdot\omega} + \frac{\omega_{pi}^2\cdot\omega_{Hi}}{((\omega - i\nu_i)^2 - \omega_{Hi}^2)\cdot\omega}, \quad \varepsilon_3 = 1 - \frac{\omega_{pe}^2}{(\omega - i\nu_e)\cdot\omega} - \frac{\omega_{pi}^2}{(\omega - i\nu_i)\cdot\omega}; \qquad (1)$$
$$\omega_{pe}^2 = \frac{4\pi e^2 n_0}{m_e}, \quad \omega_{pi}^2 = \frac{4\pi e^2 n_0}{m_i}, \quad \omega_{He} = \frac{eH_0}{m_e c}, \quad \omega_{Hi} = \frac{eH_0}{m_i c}$$

Here $\omega_{pe}, \omega_{pi}, \omega_{He}, \omega_{Hi}$ are plasma and cyclotron frequencies for electrons and ions respectively; m_e, m_i, ν_e, ν_i are the masses and the collision frequencies. The expressions of the components of $\hat{\varepsilon}(\omega,z)$ are obtained from (1) by means of multiplication with the rotation matrices (Spiegel, 1959). In the case of a medium with a scalar conductivity σ, like the lower ionosphere or atmosphere, the effective permittivity (1) reduces to the scalar: $\varepsilon = 1 - 4\pi i\sigma/\omega$.

3.2 The equations for the EM field and upper boundary conditions

The EM field depends on the horizontal coordinate x as ~$\exp(-ik_x x)$. Generally, $k_x \le k_0$, where $k_0 = \omega/c$. In simulations of VLF beam propagation, we put $k_x = k_0$. In the case of searching VLF waveguide modes k_x is slightly complex and should be calculated from boundary conditions at the Earth's surface and upper surface of the effective WGEI.

The Maxwell equations are:

Ann. Geophys. Discuss., https://doi.org/10.5194/angeo-2019-46
Manuscript under review for journal Ann. Geophys.
Discussion started: 7 May 2019

$$-\frac{\partial H_y}{\partial z}=ik_0D_x,\quad \frac{\partial H_x}{\partial z}+ik_xH_z=ik_0D_y,\quad -ik_xH_y=ik_0D_z$$
$$-\frac{\partial E_y}{\partial z}=-ik_0H_x,\quad \frac{\partial E_x}{\partial z}+ik_xE_z=-ik_0H_y,\quad -ik_xE_y=-ik_0H_z \qquad (2)$$

In eq. (2), $E_x=\beta_{11}D_x+\beta_{12}D_y+\beta_{13}D_z$ etc. All the components of the EM field can be represented through the horizontal components of the magnetic field H_x, H_y, and the following equations for these components have been derived:

$$\frac{\partial}{\partial z}\left(\frac{\beta_{22}}{1-\beta_{22}\frac{k_x^2}{k_0^2}}\frac{\partial H_x}{\partial z}\right)-\frac{\partial}{\partial z}\left(\frac{\beta_{21}}{1-\beta_{22}\frac{k_x^2}{k_0^2}}\frac{\partial H_y}{\partial z}\right)-ik_x\frac{\partial}{\partial z}\left(\frac{\beta_{23}}{1-\beta_{22}\frac{k_x^2}{k_0^2}}H_y\right)+k_0^2H_x=0 \qquad (3a)$$

$$\frac{\partial}{\partial z}\left((\beta_{11}+\frac{k_x^2}{k_0^2}\frac{\beta_{12}\cdot\beta_{21}}{1-\beta_{22}\frac{k_x^2}{k_0^2}})\frac{\partial H_y}{\partial z}\right)-\frac{\partial}{\partial z}\left(\frac{\beta_{12}}{1-\beta_{22}\frac{k_x^2}{k_0^2}}\frac{\partial H_x}{\partial z}\right)+$$
$$+ik_x\frac{\partial}{\partial z}\left((\beta_{13}+\frac{k_x^2}{k_0^2}\frac{\beta_{12}\cdot\beta_{23}}{1-\beta_{22}\frac{k_x^2}{k_0^2}})H_y\right)+ik_x(\beta_{31}+\frac{k_x^2}{k_0^2}\frac{\beta_{32}\cdot\beta_{21}}{1-\beta_{22}\frac{k_x^2}{k_0^2}})\frac{\partial H_y}{\partial z}- \qquad (3b)$$
$$-ik_x\frac{\beta_{32}}{1-\beta_{22}\frac{k_x^2}{k_0^2}}\frac{\partial H_x}{\partial z}+k_0^2(1-\beta_{33}\frac{k_x^2}{k_0^2}-\frac{k_x^4}{k_0^4}\frac{\beta_{23}\cdot\beta_{32}}{1-\beta_{22}\frac{k_x^2}{k_0^2}})H_y=0$$

The expressions for the horizontal components of the electric field E_x, E_y are:

$$E_x=\frac{i}{k_0}\left((\beta_{11}+\frac{k_x^2}{k_0^2}\frac{\beta_{12}\cdot\beta_{21}}{1-\beta_{22}\frac{k_x^2}{k_0^2}})\frac{\partial H_y}{\partial z}-\frac{\beta_{12}}{1-\beta_{22}\frac{k_x^2}{k_0^2}}\frac{\partial H_x}{\partial z}\right)-\frac{k_x}{k_0}(\beta_{13}+\frac{k_x^2}{k_0^2}\frac{\beta_{12}\cdot\beta_{23}}{1-\beta_{22}\frac{k_x^2}{k_0^2}})H_y$$

$$E_y=\frac{i}{k_0}\left(-\frac{\beta_{22}}{1-\beta_{22}\frac{k_x^2}{k_0^2}}\frac{\partial H_x}{\partial z}+\frac{\beta_{21}}{1-\beta_{22}\frac{k_x^2}{k_0^2}}\frac{\partial H_y}{\partial z}\right)-\frac{k_x}{k_0}\frac{\beta_{23}}{1-\beta_{22}\frac{k_x^2}{k_0^2}}H_y \qquad (4)$$

In the region $z \geq L_{max}$ the upper ionosphere is assumed weakly inhomogeneous, and the geometric optics approximation is valid in the VLF range there. Note that such an approximation is invalid at the upper boundary of the effective VLF WGEI at 80 – 90 km because of the great inhomogeneity of the ionosphere in the vertical direction within *E*-layer. These circumstances determine the choice of the upper boundary $z = L_{max} \sim$ (250-400) km, where the conditions of the radiation are

Ann. Geophys. Discuss., https://doi.org/10.5194/angeo-2019-46
Manuscript under review for journal Ann. Geophys.
Discussion started: 7 May 2019

formulated. The dispersion equation connected the wave numbers and the frequency of the outgoing waves has been got from eqs. (3), where $H_{x,y} \sim e^{-ik_z\tilde{z}}$, while the derivatives like $\partial\beta_{11}/\partial z$ and the inhomogeneity of the media are neglected:

$$\left(\beta_{22}k_z^2 - k_0^2(1-\beta_{22}\frac{k_x^2}{k_0^2})\right)\cdot\left((\beta_{11}(1-\beta_{22}\frac{k_x^2}{k_0^2})+\frac{k_x^2}{k_0^2}\beta_{12}\cdot\beta_{21})k_z^2+((\beta_{13}+\beta_{31})(1-\beta_{22}\frac{k_x^2}{k_0^2})+\right.$$
$$\left.+\frac{k_x^2}{k_0^2}(\beta_{12}\cdot\beta_{23}+\beta_{32}\cdot\beta_{21})k_xk_z - k_0^2((1-\beta_{33}\frac{k_x^2}{k_0^2})(1-\beta_{22}\frac{k_x^2}{k_0^2})-\frac{k_x^4}{k_0^4}\beta_{23}\cdot\beta_{32})\right)- \quad (5)$$
$$-\left(\beta_{21}k_z^2+\beta_{23}k_xk_z\right)\cdot\left(\beta_{12}k_z^2-\beta_{32}k_xk_z\right)=0$$

Thus, generally Eq. (5) which determines the wave numbers for the outgoing waves is of the 4th order (Weit 1996). The boundary conditions at the upper boundary $z = L_{max}$ within the ionosphere F-layer are the absence of the ingoing waves, i.e. the outgoing (radiated) waves are present only. Two roots should be selected that possess the negative imaginary parts $Im(k_{z1,z2}) < 0$, i.e. the outgoing waves dissipate upwards. But in the case of VLF waves some simplification can be used. Namely, the expressions for the wave numbers $k_{1,2}$ are obtained from eqs. (3), where the dependence on x is neglected: $|k_{1,2}| >> k_0$. This approximation is valid within F-layer where the first outgoing wave corresponds to the whistler of small dissipation, the second one to the highly dissipating slow wave. The EM field components, which are necessary to formulate the boundary conditions for eqs. (3a, b) at $z \geq L_{max}$, can be presented as:

$$H_x = A_1e^{-ik_{z1}\tilde{z}} + \alpha_2A_2e^{-ik_{z2}\tilde{z}}, \quad H_y = \alpha_1A_1e^{-ik_{z1}\tilde{z}} + A_2e^{-ik_{z2}\tilde{z}} \quad (6)$$

In the relations (6), $\tilde{z} = z - L_z$. eqs. (3) are simplified there in the approximation described above:

$$\beta_{22}\frac{\partial^2H_x}{\partial z^2} - \beta_{21}\frac{\partial^2H_y}{\partial z^2} + k_0^2H_x = 0,\ \beta_{11}\frac{\partial^2H_y}{\partial z^2} - \beta_{12}\frac{\partial^2H_x}{\partial z^2} + k_0^2H_y = 0 \quad (7)$$

Again, the solution of eqs. (7) is searched as: $H_{x,y} \sim e^{-ik_z\tilde{z}}$. The following equation has been obtained to get the wave numbers $k_{z1,z2}$ from eqs. (7):

$$\kappa^4 - (\beta_{22}+\beta_{11})\kappa^2 + \beta_{11}\beta_{22} - \beta_{12}\beta_{21} = 0, \quad \kappa^2 = \frac{k_0^2}{k_z^2} \quad (8)$$

Therefore as it follows from eq. (8),

$$\kappa_{1,2}^2 = \frac{\beta_{11}+\beta_{22}}{2} \pm \left((\frac{\beta_{11}+\beta_{22}}{2})^2 + \beta_{12}\beta_{21}\right)^{1/2};\ \alpha_1 = \frac{\beta_{22}-\kappa_1^2}{\beta_{21}} = \frac{\beta_{12}}{\beta_{11}-\kappa_1^2};\ \alpha_2 = \frac{\beta_{11}-\kappa_2^2}{\beta_{12}} = \frac{\beta_{21}}{\beta_{22}-\kappa_2^2};\ k_{z1,z2}^2 = \frac{k_0^2}{\kappa_{1,2}^2} \quad (9)$$

The signs of $k_{z1,z2}$ have been chosen from the condition $Im(k_{z1,z2}) < 0$. From Eqs. (5) at the upper boundary $z = L_{max}$ the following relations are valid:

$$H_x = A_1 + \alpha_2A_2, \quad H_y = \alpha_1A_1 + A_2 \quad (10)$$

As it follows from eq. (10),

$$A_1 = \Delta^{-1}(H_x - \alpha_2H_y);\ A_2 = \Delta^{-1}(H_y - \alpha_1H_x);\ \Delta = 1 - \alpha_1\alpha_2 \quad (11)$$

Ann. Geophys. Discuss., https://doi.org/10.5194/angeo-2019-46
Manuscript under review for journal Ann. Geophys.
Discussion started: 7 May 2019

Annales Geophysicae Discussions

Thus, it is possible to exclude the amplitudes of the outgoing waves $A_{1,2}$ from Eqs. (9). As a result, at $z = L_{max}$ the boundary conditions are rewritten in terms of H_x, H_y only:

$$\frac{\partial H_x}{\partial z} = -i(k_{z1}A_1 + k_{z2}\alpha_2 A_2) = -\frac{i}{\Delta}\left((k_{1z} - \alpha_1\alpha_2 k_{z2})H_x + \alpha_2(k_{z2} - k_{z1})H_y\right)$$
$$\frac{\partial H_y}{\partial z} = -i(k_{z1}\alpha_1 A_1 + k_{z2}A_2) = -\frac{i}{\Delta}\left((k_{z2} - \alpha_1\alpha_2 k_{z1})H_y + \alpha_1(k_{z1} - k_{z2})H_x\right) \quad (12)$$

The relations (12) are the upper boundary conditions of the radiation for the boundary $z=L_{max}$~(250-400) km. Then these conditions will be transformed/recalculated using the analytical-numerical recurrent procedure into equivalent impedance boundary conditions at $z=L_z$~(70-90) km.

Note that in the "whistler/VLF approximation", valid at frequencies ~ 10 kHz, one can get for the F region of the ionosphere**.** In this approximation and accounting for that $k_x \approx 0$, we find, using eqs. (5), (8), (9) that dispersion equation takes the form

$$k_z'^2 k^2 = k_0^2 g^2 \quad (13)$$

where $k^2 = k_x^2 + k_z^2 = k_x'^2 + k_z'^2$; k_x' and k_z' are the components of wave number, transverse and longitudinal respectively to geomagnetic field, respectively. For the F region of the ionosphere, where $\nu_e << \omega << \omega_{He}$, eq. (13) reduces to the standard form of whistler dispersion equation $|k_z'|k = k_0|g|$; $g \approx -\omega_{pe}^2/(\omega\omega_{He})$; $\omega = c^2 k |k_z'|/(\omega_{He}/\omega_{pe}^2)$; in a special case of the waves, propagating exactly along geomagnetic field, $k_x' = 0$, one obtain, for the propagating whistler waves, well-known dispersion dependence (Artcimovich and Sagdeev, 1979) $\omega = c^2 k_z'^2(\omega_{He}/\omega_{pe}^2)$. Coming back to our problem and accounting for that in our case we can reasonably put $k_x \approx 0$, eq. (13) reduces to $k_z^4 \cos^2\theta = k_0^4 g^2$. As a result, we get $k_{z1} = \sqrt{g/\cos\theta}k_0$, $k_{z2} = -i\sqrt{g/\cos\theta}k_0$, and then, similarly to the relations (12), the boundary conditions can be presented, in terms of the tangential components of electric field, particularly in the form:

$$\frac{\partial \vec{U}}{\partial z} + \hat{B}\vec{U} = 0;\ \vec{U} = \begin{bmatrix} E_x \\ E_y \end{bmatrix};\ \hat{B} = \frac{1}{2}\sqrt{\frac{g}{\cos\theta}}k_0 \begin{bmatrix} 1+i & 1-i \\ 1+i & 1+i \end{bmatrix} \quad (14)$$

Conditions (12) or (14) are the conditions of radiation (absence of ingoing waves) formulated at the upper boundary $z=L_{max}$ and suitable for the determination of the energy of the wave leaking from the WGEI into the upper ionosphere/magnetosphere. Let us emphasize again that the formulas expressing the boundary conditions of the radiation (more accurately speaking, an absence of incoming waves, what is the consequence to the causality principle) (12), (14) are obtained as a result of limiting pass by the small parameter $k_x/k_0 \,|\, k_x/k_z| \to 0$ in eq. (5). Note that in spite of disappearance of the dependence of these boundary conditions explicitly on k_x, the dependence of the characteristics of the wave propagation process on k_x, as a whole, is accounted for, and all results are still valid for the description of the wave beam propagation in the WGEI along the horizontal axis x with finite $k_x \sim k_0$.

Ann. Geophys. Discuss., https://doi.org/10.5194/angeo-2019-46
Manuscript under review for journal Ann. Geophys.
Discussion started: 7 May 2019

3.3 Equivalent Tensor Impedance Boundary Conditions at the Upper Boundary $z=L_z$ of the Effective WGEI

The tensor impedance at the upper boundary of the effective WGEI $z=L_z$, Fig. 1, is obtained by means of recalculating to the level $z=L_z\sim$ 80 – 90 km of the conditions of radiation (12) or (14), formulated at the upper boundary, placed in the F region of the ionosphere, at $z=L_{max}\sim$ (250-400) km.

The main idea of the effective tensor impedance method is the unification of the analytical and numerical approaches and the derivation of the proper impedance boundary conditions without any approximation of the "thin cover layer", used in the majority of an effective impedance approaches previously, applied either for artificial or natural layered gyrotropic structures, see, f.e. (Tretyakov, 2003; Senior and Volakis, 1995; Kurushin and Nefedov, 1983; Alperovich and Fedorov, 2007). There is one known exception, namely invariant imbedding impedance method (Shalashov and Gospodchikov, 2010; Kim and Kim, 2016)..The comparison of our method with the invariant imbedding impedance method will be presented in the end of this subsection. Eqs. (3), jointly with the boundary conditions (12), have been solved by finite differences. Outline here the main ideas and the steps of the derivations of the corresponding formulas.

The derivatives in Eqs. (3) are approximated as

$$\frac{\partial}{\partial z}\left(C(z)\frac{\partial H_x}{\partial z}\right)\approx\frac{1}{h}\left(C(z_{j+1/2})\frac{(H_x)_{j+1}-(H_x)_j}{h}-C(z_{j-1/2})\frac{(H_x)_j-(H_x)_{j-1}}{h}\right),$$
$$\frac{\partial}{\partial z}\left(F(z)H_x\right)\approx\frac{1}{2h}\left(F(z_{j+1})(H_x)_{j+1}-F(z_{j-1})(H_x)_{j-1}\right)\quad\text{etc.} \tag{15}$$

In eq. (15), $z_{j+1/2}=h\cdot(j+0.5)$. In eqs. (10) the approximation is $\partial H_x/\partial z\approx[(H_x)_N-(H_x)_{N-1}]/h$. Here h is the discretization step along OZ axis, N is the total number of the nodes. At each step j the difference approximations of Eqs. (3) take the form:

$$\hat{\alpha}_j^{(-)}\cdot\vec{H}_{j-1}+\hat{\alpha}_j^{(0)}\cdot\vec{H}_j+\hat{\alpha}_j^{(+)}\cdot\vec{H}_{j+1}=0 \tag{16}$$

where $\vec{H}_j=\begin{pmatrix}H_x\\H_y\end{pmatrix}$, $j=N-1,N-2,...,1$, $z_j=h\cdot j$, $L_z=h\cdot N$. The expressions for the matrix coefficients in Eq. (16) are complicated; they are given in Appendix. The set of the matrix eqs. (16) has been solved by the method called factorization, or elimination, or matrix sweep (method) [Samarskii, 2001]. Namely, it is possible to write down:

$$\vec{H}_j=\hat{b}_j\cdot\vec{H}_{j-1},\quad j=N,...,1 \tag{17a}$$

$$H_{xj+1}=b_{11j+1}H_1+b_{12j+1}H_2;\ H_{yj+1}=b_{21j+1}H_1+b_{22j+1}H_2;\ H_1\equiv H_{xj};\ H_2\equiv H_{yj} \tag{17b}$$

This method is in fact a variant of the Gauss elimination method for the matrix 3-diagonal set of the Eqs. (16). The value of $\hat{b}_N$ has been obtained from the boundary conditions (12). Namely, they can be rewritten as:

Ann. Geophys. Discuss., https://doi.org/10.5194/angeo-2019-46
Manuscript under review for journal Ann. Geophys.
Discussion started: 7 May 2019

$$\hat{\alpha}_N^{(-)} \cdot \vec{H}_{N-1} + \hat{\alpha}_N^{(0)} \cdot \vec{H}_N = 0 \quad (18)$$

Therefore $\hat{b}_N = -(\hat{\alpha}_N^{(0)})^{-1} \cdot \hat{\alpha}_N^{(-)}$. Then the matrices $\hat{b}_j$ have been computed sequentially down till the desired value of $z = L_z = h \cdot N_z$, where the impedance boundary conditions are assumed to be applied. At each step the formulas for $\hat{b}_j$ follow from (16), (17) and take the form

$$(\hat{\alpha}_j^{(0)} + \hat{\alpha}_j^{(+)} \cdot \hat{b}_{j+1}) \cdot \vec{H}_j = -\hat{\alpha}_j^{(-)} \cdot \vec{H}_{j-1} \quad (19)$$

Therefore accounting for (17), we obtain $\hat{b}_j = -(\hat{\alpha}_j^{(0)} + \hat{\alpha}_j^{(+)} \cdot \hat{b}_{j+1})^{-1} \cdot \hat{\alpha}_j^{(-)}$. The derivatives in eqs. (4) have been approximated as:

$$(\frac{\partial H_x}{\partial z})_{N_z} \approx \frac{(H_x)_{N_z+1} - (H_x)_{N_z}}{h} = \frac{(b_{N_z+1\ \ 11} - 1) \cdot (H_x)_{N_z} + b_{N_z+1\ \ 12} \cdot (H_y)_{Nz}}{h} \text{; analogously for } (\frac{\partial H_y}{\partial z})_{N_z} \quad (20)$$

Note that a result of this discretization, only the values at the grid level N_z are included into the numerical approximation of the derivatives $\partial H_{x,y} / \partial z$ at $z = L_z$. We determine tensor impedance $\hat{Z}$ in particular at $z=L_z \sim 85$ km such as the tensor value containing in the following relations, all of which are related to the corresponding altitude (in other words, to the grid with number N_z, corresponding to this altitude):

$$\vec{n} \times \vec{E} = \hat{Z} \cdot \vec{H},\ \vec{n} = (0,0,1);\ \text{or}\ E_x = Z_{21} H_x + Z_{22} H_y;\ E_y = -Z_{11} H_x - Z_{12} H_y \quad (21)$$

The equivalent tensor impedance is obtained, in fact, using two-step procedure. (1) We obtain the matrix $\hat{b}_j$ using the set of equations (3a, b) with the boundary conditions (12) and the procedure (17)-(19) described above. (2) Put the expressions (21) with tensor impedance into the left parts and the derivatives $\partial H_{x,y} / \partial z$ in the form (20) into the right parts of eqs. (4). Equating in the left and right parts of the two obtained equations coefficients at H_x, H_y respectively, we obtain the analytical expressions for the components of the tensor impedance at $z = L_z$:

$$Z_{11} = -\frac{i}{k_0 h}\left(\frac{\beta_{21}}{1-\beta_{22}\frac{k_x^{\ 2}}{k_0^{\ 2}}} \cdot b_{21} - \frac{\beta_{22}}{1-\beta_{22}\frac{k_x^{\ 2}}{k_0^{\ 2}}} \cdot (b_{11}-1)\right),\ Z_{12} = -\frac{i}{k_0 h}\left(\frac{\beta_{21}}{1-\beta_{22}\frac{k_x^{\ 2}}{k_0^{\ 2}}}\frac{\partial H_y}{\partial z} \cdot (b_{22}-1) - \frac{\beta_{22}}{1-\beta_{22}\frac{k_x^{\ 2}}{k_0^{\ 2}}} \cdot b_{12} - k_x h \cdot \frac{\beta_{23}}{1-\beta_{22}\frac{k_x^{\ 2}}{k_0^{\ 2}}}\right),$$

$$Z_{21} = \frac{i}{k_0 h}\left((\beta_{11} + \frac{k_x^{\ 2}}{k_0^{\ 2}}\frac{\beta_{12} \cdot \beta_{21}}{1-\beta_{22}\frac{k_x^{\ 2}}{k_0^{\ 2}}}) \cdot b_{21} - \frac{\beta_{12}}{1-\beta_{22}\frac{k_x^{\ 2}}{k_0^{\ 2}}} \cdot (b_{11}-1)\right),$$

Ann. Geophys. Discuss., https://doi.org/10.5194/angeo-2019-46
Manuscript under review for journal Ann. Geophys.
Discussion started: 7 May 2019

Annales Geophysicae Discussions Open Access EGU

$$Z_{22}=\frac{i}{k_0 h}\left((\beta_{11}+\frac{k_x^{\,2}}{k_0^{\,2}}\frac{\beta_{12}\cdot\beta_{21}}{1-\beta_{22}\frac{k_x^{\,2}}{k_0^{\,2}}})\cdot(b_{22}-1)-k_x h\cdot(\beta_{13}+\frac{k_x^{\,2}}{k_0^{\,2}}\frac{\beta_{12}\cdot\beta_{23}}{1-\beta_{22}\frac{k_x^{\,2}}{k_0^{\,2}}})-\frac{\beta_{12}}{1-\beta_{22}\frac{k_x^{\,2}}{k_0^{\,2}}}\cdot b_{12}\right) \quad (22)$$

The proposed method of the transfer of the boundary conditions from the ionosphere *F*-layer L_{max} = 250 – 400 km into the lower part of the *E*-layer L_z =80 – 90 km is stable and easily realizable, when compared with some alternative approaches based on the invariant imbedding methods (Shalashov and Gospodchikov, 2010; Kim and Kim, 2016). The stability of our method is due to the stability of the Gauss elimination method when the coefficients at the central diagonal are dominating; the last is valid for the ionosphere with electromagnetic losses where the absolute values of the permittivity tensor are big. The application of the proposed method of the matrix sweep in the media without losses may require the utilization of the Gauss method with the choice of the maximum element, to ensure the stability. But, as our simulations (not presented here) demonstrated, for the electromagnetic problems in the frequency domain the simple Gauss elimination and one with the choice of the maximal element gives the same results. The accumulation of errors may occur in evolutional problems in the time domain, when the Gauss method should be applied sequentially many times. The use of the independent functions H_x, H_y in Eqs. (3) seems natural, as well as the transfer (17a), because the impedance conditions are the expressions of the electric E_x, E_y through these magnetic components H_x, H_y at the upper boundary of the VLF waveguide 80 – 90 km. The naturally chosen direction of the recalculation of the upper boundary conditions from $z=L_{max}$ to $z=L_z$, i.e from upper layer with large impedance value to lower altitude layer with relatively small impedance value, provides, at the same time, the stability of the simulation procedure. The obtained components of the tensor impedance are small, $|Z_{\alpha\beta}| \leq 0.1$. This determines the choice of the upper boundary $z=L_z$ of the effective WGEI. Due to small enough impedance, EM waves incident from below on this boundary reflect effectively back. Therefore, the region $0 \leq z \leq L_z$ indeed can be presented as an effective WGEI. Then such a waveguide includes not only lower up to L_{ISO} ~ (65-75) km with rather small losses, but also thin dissipative and anisotropic/gyrotropic layer between 75 and 85-90 km.

Finally, the main differences and at the same time advantages of the proposed tensor impedance method from the known method of the impedance recalculating, in particular invariant imbedding methods (Shalashov and Gospodchikov, 2010; Kim and Kim, 2016) are the following. (i) In distinction to invariant imbedding method, our method is a direct method of the recalculation of tensor impedance, and the corresponding tensor impedance is determined analytically, see eqs. (22). (ii) Our method, for the media without non-locality, does not need a solution of integral equation(s), as in invariant imbedding method. (iii) The proposed tensor impedance method does not need the revealing of forward and reflected waves. Moreover, even the conditions of the radiation (12) at the upper boundary $z=L_{max}$ are determined through the total field components $H_{x,y}$, what makes the proposed procedure technically much less cumbersome and practically much more convenient. (iv) At the same time, the procedure is very effective and computationally stable, as it is explained above in this subsection. As it is already mentioned, for the very low-loss systems, the required level of stability can be achieved with the modification based on the choice of the maximal element for matrix inversion.

Ann. Geophys. Discuss., https://doi.org/10.5194/angeo-2019-46
Manuscript under review for journal Ann. Geophys.
Discussion started: 7 May 2019

3.4 Propagation of the Electromagnetic Waves in the Gyrotropic Waveguide and the TIMEB Method

Use, as the independent functions, the transverse components E_y, H_y. The goal is to derive the equations for the slowly varying amplitudes *A(x,y,z), B(x,y,z)* of the VLF beams included corresponding field components:

$$E_y = \frac{1}{2}A(x,y,z)\cdot e^{i\omega t - ik_0 x} + c.c., \quad H_y = \frac{1}{2}B(x,y,z)\cdot e^{i\omega t - ik_0 x} + c.c. \tag{23}$$

Note that in this case it should be $k_x = k_0$, because the beam propagates in the WGEI, the main part of which is occupied by the atmosphere and lower ionosphere (D region), rather closed to free space by its electromagnetic parameters. The presence of a thin anisotropic and dissipative layer belonging to the E region of the ionosphere causes, altogether with the impedance boundary condition the proper z dependence of *B(x,y,z)*. Using (21), (22), it is possible to write down the boundary conditions at the height $z = L_z$ for the slowly varying amplitudes *A(x,y,z), B(x,y,z)* of the transverse components E_y, H_y. Namely, from the Maxwell equations in the method of beams it is possible to express the components E_x and H_x through E_y, H_y:

$$H_x \approx -\frac{i}{k_0}\frac{\partial E_y}{\partial z}, \quad E_x \approx \gamma_{12}E_y + i\frac{\tilde{\beta}_{33}}{k_0}\frac{\partial H_y}{\partial z} + \tilde{\beta}_{13}H_y \tag{24}$$

where $\gamma_{12} = \Delta^{-1}(\varepsilon_{13}\varepsilon_{32} - \varepsilon_{12}\varepsilon_{33})$, $\tilde{\beta}_{13} = \Delta^{-1}\varepsilon_{13}$, $\tilde{\beta}_{33} = \Delta^{-1}\varepsilon_{33}$; $\Delta = \varepsilon_{11}\varepsilon_{33} - \varepsilon_{13}\varepsilon_{31}$. The using of Eqs. (21) and (24) leads to the following form of the boundary conditions for *A, B*:

$$A - \frac{i}{k_0}Z_{11}\cdot\frac{\partial A}{\partial z} + Z_{12}\cdot B \approx 0, \quad \gamma_{12}\cdot A + \frac{i}{k_0}Z_{21}\cdot\frac{\partial A}{\partial z} + (\tilde{\beta}_{13} - Z_{22})\cdot B + \frac{i}{k_0}\tilde{\beta}_{33}\cdot\frac{\partial B}{\partial z} \approx 0 \tag{25}$$

Let us derive the evolution equations for the slowly varying amplitudes *A(x,y,z), B(x,y,z)* of the VLF beams. Below the monochromatic beams are considered, so the frequency ω is fixed and the amplitudes do not depend on time t. Search the solutions for the EM field as $\vec{E},\vec{H} \sim \exp(i\omega t - ik_x x - ik_y y)$. The Maxwell equations are written down as

$$\begin{aligned} &-ik_y H_z - \frac{\partial H_y}{\partial z} = ik_0 D_x, \quad \frac{\partial H_x}{\partial z} + ik_x H_z = ik_0 D_y, \quad -ik_x H_y + ik_y H_x = ik_0 D_z \\ &-ik_y E_z - \frac{\partial E_y}{\partial z} = -ik_0 H_x, \quad \frac{\partial E_x}{\partial z} + ik_x E_z = -ik_0 H_y, \quad -ik_x E_y + ik_y E_x = -ik_0 H_z \end{aligned} \tag{26}$$

Here $D_x = \varepsilon_{11}E_x + \varepsilon_{12}E_y + \varepsilon_{13}E_z$. From Eqs. (21) it is possible to get the expressions for E_x, E_z through E_y, H_y:

$$\begin{aligned} E_x &= \frac{1}{\Delta}\left\{[\varepsilon_{13}\cdot\varepsilon_{32} - (\varepsilon_{12} + \frac{k_x k_y}{k_0^2})\cdot(\varepsilon_{33} - \frac{k_y^2}{k_0^2})]E_y + \frac{i}{k_0}(\varepsilon_{33} - \frac{k_y^2}{k_0^2})\frac{\partial H_y}{\partial z} + \frac{k_x}{k_0}\varepsilon_{13}\cdot H_y + \frac{ik_y}{k_0^2}\varepsilon_{13}\frac{\partial E_y}{\partial z}\right\} \\ E_z &= \frac{1}{\Delta}\left\{[\varepsilon_{31}\cdot(\varepsilon_{12} + \frac{k_x k_y}{k_0^2}) - \varepsilon_{32}\cdot(\varepsilon_{11} - \frac{k_y^2}{k_0^2})]E_y - \frac{i}{k_0}\varepsilon_{31}\frac{\partial H_y}{\partial z} - \frac{k_x}{k_0}\cdot(\varepsilon_{11} - \frac{k_y^2}{k_0^2})H_y - \frac{ik_y}{k_0^2}\cdot(\varepsilon_{11} - \frac{k_y^2}{k_0^2})\frac{\partial E_y}{\partial z}\right\} \end{aligned} \tag{27}$$

In eq. (27), $\Delta \equiv (\varepsilon_{11} - \frac{k_y^2}{k_0^2})\cdot(\varepsilon_{33} - \frac{k_y^2}{k_0^2}) - \varepsilon_{31}\cdot\varepsilon_{13}$. The equations for E_y, H_y obtained from the Maxwell equations are:

Ann. Geophys. Discuss., https://doi.org/10.5194/angeo-2019-46
Manuscript under review for journal Ann. Geophys.
Discussion started: 7 May 2019

$$\left(\frac{\partial^2}{\partial z^2}-k_x{}^2-k_y{}^2\right)E_y+ik_y\left(\frac{\partial E_z}{\partial z}-ik_xE_x-ik_yE_y\right)+k_0{}^2D_y=0;\ -ik_0\frac{\partial E_x}{\partial z}+k_xk_0E_z+k_0{}^2H_y=0 \tag{28}$$

After substitution of expressions (27) for for E_x, E_z into Eqs. (28) the coupled equations for E_y, H_y only can be got. Namely, the expansion should be used: $k_x = k_0 + \delta k_x$, $|\delta k_x| << k_0$, also $|k_y| << k_0$. Then the correspondence should be applied (Weiland and Wilhelmsson 1977):

$$-i\cdot\delta k_x\to\frac{\partial}{\partial x},\ -i\cdot k_y\to\frac{\partial}{\partial y} \tag{29}$$

The expansions should be till the quadratic terms with respect to k_y and the linear terms with respect to δk_x. As a result, the parabolic equations (Levy 2000) for the slowly varying amplitudes A and B have been derived. In the atmosphere and the lower ionosphere, where the effective permittivity reduces to a scalar $\varepsilon(\omega,z)$, they are independent:

$$\begin{aligned}&\frac{\partial A}{\partial x}+\frac{i}{2k_0}\left(\frac{\partial^2 A}{\partial y^2}+\frac{\partial^2 A}{\partial z^2}\right)+\frac{ik_0}{2}\cdot(\varepsilon-1)A=0\\&\frac{\partial B}{\partial x}+\frac{i}{2k_0}\left(\frac{1}{\beta}\frac{\partial}{\partial z}(\beta\frac{\partial B}{\partial z})+\frac{\partial^2 B}{\partial y^2}\right)+\frac{ik_0}{2}\cdot(\varepsilon-1)B=0\end{aligned} \tag{30a}$$

Here $\beta\equiv\varepsilon^{-1}$. Accounting for the presence of gyrotropic layer near the and the presence of tensor impedamce boundary conditions at the upper boundary $z = L_z$ of the VLF waveguide, the equations for the slowly varying amplitudes in general case are coupled and possess a complicated form:

$$\begin{aligned}&\frac{\partial A}{\partial x}+\frac{i}{2k_0}\left(\frac{\partial^2 A}{\partial y^2}+\frac{\partial^2 A}{\partial z^2}\right)+\frac{ik_0}{2}\cdot(\tilde{\varepsilon}_{22}-1)\cdot A+\frac{\gamma_{21}}{2}\frac{\partial B}{\partial z}+\frac{ik_0}{2}\cdot\gamma_{23}B=0\\&\frac{\partial B}{\partial x}+\frac{i}{2k_0}\left(\frac{1}{\tilde{\beta}_{11}}\frac{\partial}{\partial z}(\tilde{\beta}_{33}\frac{\partial B}{\partial z})+\frac{\partial^2 B}{\partial y^2}\right)+\frac{i}{2\tilde{\beta}_{11}}\frac{\partial}{\partial z}(\gamma_{12}A)+\frac{1}{2\tilde{\beta}_{11}}\frac{\partial}{\partial z}(\tilde{\beta}_{13}B)+\frac{ik_0}{2\tilde{\beta}_{11}}\gamma_{32}A+\frac{\tilde{\beta}_{31}}{2\tilde{\beta}_{11}}\frac{\partial B}{\partial z}+\frac{ik_0}{2}\cdot(\frac{1}{\tilde{\beta}_{11}}-1)\cdot B=0\end{aligned} \tag{30b}$$

In Eq. (30b),

$$\gamma_{12}\equiv\frac{\varepsilon_{13}\cdot\varepsilon_{32}-\varepsilon_{12}\cdot\varepsilon_{33}}{\Delta},\gamma_{21}\equiv\frac{\varepsilon_{23}\cdot\varepsilon_{31}-\varepsilon_{21}\cdot\varepsilon_{33}}{\Delta},\gamma_{23}\equiv\frac{\varepsilon_{21}\cdot\varepsilon_{13}-\varepsilon_{23}\cdot\varepsilon_{11}}{\Delta},\gamma_{32}\equiv\frac{\varepsilon_{31}\cdot\varepsilon_{12}-\varepsilon_{32}\cdot\varepsilon_{11}}{\Delta},\tilde{\beta}_{11}\equiv\frac{\varepsilon_{11}}{\Delta},\tilde{\beta}_{13}\equiv\frac{\varepsilon_{13}}{\Delta},$$

$$\tilde{\beta}_{31}\equiv\frac{\varepsilon_{31}}{\Delta},\tilde{\beta}_{33}\equiv\frac{\varepsilon_{33}}{\Delta};\Delta\equiv\varepsilon_{11}\cdot\varepsilon_{33}-\varepsilon_{13}\cdot\varepsilon_{31}.$$

Eqs. (30b) reduce to Eqs. (30a) when the effective permittivity is scalar. At the Earth's surface $z = 0$ the impedance conditions reduce, due to a finite conductivity of the Earth, to the form:

$$E_y=Z_EH_x,\quad E_x=-Z_EH_y,\quad Z_E\equiv\left(\frac{i\omega}{4\pi\sigma_E}\right)^{1/2} \tag{31a}$$

Ann. Geophys. Discuss., https://doi.org/10.5194/angeo-2019-46
Manuscript under review for journal Ann. Geophys.
Discussion started: 7 May 2019

Annales Geophysicae Discussions Open Access EGU

Here $\sigma_E \sim 10^8$ s^{-1} is the Earth's conductivity. The boundary conditions (31a) at the Earth's surface, where $Z_{22} = Z_{21} \equiv Z_E$, $Z_{12} = Z_{21} = 0$, $\beta_{33} = \varepsilon(z=0)^{-1}$, $\gamma_{12} = 0$, $\tilde{\beta}_{13} = 0$, can be rewritten as

$$E_y + \frac{i}{k_0} Z_E \frac{\partial E_y}{\partial z} = 0, \quad \frac{i}{\varepsilon(z=0) k_0} \frac{\partial H_y}{\partial z} + \frac{i}{k_0} Z_E H_y = 0 \tag{31b}$$

The Eqs. (30) added by the boundary conditions (25) at the upper boundary of the VLF waveguide $z=L_z$ and by the boundary conditions at the Earth's surface (31b) are used below to simulate the VLF wave propagation. The surface impedance of the Earth has been calculated from the Earth's conductivity. The initial conditions to the problem (30), (25), (31b) are

$$A(x=0,y,z) = 0,\ B(x=0,y,z) = B_0 exp\left(-\left(\left(y-0.5L_y\right)/y_0\right)^{2n}\right) exp\left(-\left(\left(z-z_1\right)/z_0\right)^{2n}\right),\ n = 2 \tag{32}$$

The size of the computing region along OY axis is $L_y \sim 1000$ km. Because the gyrotropic layer is relatively thin and is placed at the upper part of the VLF waveguide, whereas the beams are excited near the Earth's surface, the wave diffraction in this gyrotropic layer along OY axis is quite small, i.e. the terms with $\partial^2 A/dy^2$, $\partial^2 B/dy^2$ are small there. Contrary to this, the wave diffraction is very important in the atmosphere in the lower part of the VLF waveguide near the Earth's surface. To solve the problem of the beam propagation, the method of splitting with respect to physical factors has been applied (Samarskii 2001). Namely, the problem has been approximated by the finite differences:

$$\vec{C} \equiv \begin{pmatrix} A \\ B \end{pmatrix}, \quad \frac{\partial \vec{C}}{\partial x} + \hat{L}_y \vec{C} + \hat{L}_z \vec{C} = 0 \tag{33}$$

In the terms $\hat{L}_y \vec{C}$ the derivatives with respect to y are included, whereas all another terms are included into $\hat{L}_z \vec{C}$. Then the following fractional steps have been applied, the 1st one is along y, the 2nd one is along z:

$$\frac{\vec{C}^{p+1/2} - \vec{C}^{p}}{h_x} + \hat{L}_y \vec{C}^{p+1/2} = 0, \quad \frac{\vec{C}^{p+1} - \vec{C}^{p+1/2}}{h_x} + \hat{L}_z \vec{C}^{p+1} = 0 \tag{34}$$

The region of simulation is $0 < x < Lx = 1000 - 2000$ km, $0 < y < L_y = 2000 - 3000$ km, $0 < z < L_z = 80 - 90$ km. The numerical scheme (34) is absolutely stable. Here h_x is the step along OX axis, $x_p = p\ h_x$, $p = 0,1,2,\ldots$. This step has been chosen from the condition of the independence of the simulation results on diminishing h_x.

Ann. Geophys. Discuss., https://doi.org/10.5194/angeo-2019-46
Manuscript under review for journal Ann. Geophys.
Discussion started: 7 May 2019

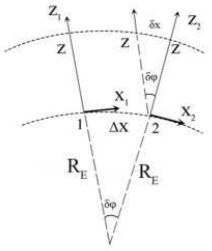

Figure 2. The rotation of the local Cartesian coordinate frame at each step along the Earth's surface h_x. on a small angle $\delta\varphi \approx \approx \Delta x/R_E$, radians, while $\Delta x=h_x$. The following strong inequalities are valid $h_x << L_z << R_E$. The Earth's surface is at $Z = 0$.

Under the simulations at each step along *OX* axis the correction due to the Earth's curvature has been inserted in adiabatic manner, namely the rotation of the local coordinate frame *XOZ*. Because the step along x is small $h_x \sim 1$ km $<< L_i$, this correction of the $\vec{C}$ results in the multiplier $exp(-ik_0 \cdot \delta x)$, where $\delta x = z \cdot (h_x/R_E)$, $R_E >> L_i$ is the Earth's radius, see Fig. 2 and the capture to this figure. At the distances $x \leq 1000$ km the results of simulations do not depend on the insertion of this correction, whereas at higher distances some quantitative differences occur. Namely, the VLF beam propagates more closely to the upper boundary of the waveguide.

3.5 The Modes of the VLF Waveguide. Reflection from the Upper Effective Boundary of VLF Waveguide and Leakage Modes: Idea of Synthetic Full Wave Electromagnetic-Complex Geometrical Optics (FWEM-CGO) Approach for Magnetized Plasma

Our model, in general, needs the consideration of the excitations of the waveguide modes by means of current sources such as dipole-like VLF radio source and lightning discahrges. Then, we will present the results of the reflection of the waves incident on the upper boundary ($z=L_z$) of the effective WGEI demonsrtrating that this structure has indeed good enough waveguiding properties. Then, in the model described in the present paper, the VLF beam is postulated already on the input of the system. To understand, how such a beam is excited by the, say, dipole antenna near the lower boundary $z=0$ of the WGEI, the formation of the beam structure on the basis of the mode presentation should be searched. Then the conditions of the radiation (absence of ingoing waves) (12) can be used as the boundary conditiuons for the VLF beam radiated to the upper ionosphere/magnetosphere. Due to relatively large scale of the inhomogeneity in this region, the complex geometrical optics (Rapoport et al. 2014) would be quite suitable for the modeling a beam propagation, even accounting for the wave dispersion in magnetized plasma. The proper effective boundary condition, similarly to (Rapoport et al. 2014) would allow to make relatively accurate matching between the regions, described by means of full wave electromagnetic approach (with Maxwell equations) and complex geometrical optics (FWEM-CGO approach). All of these material is not included into the presenbt paper, but will be delivered in the two future papers, one of which will be dedicated, shortly spealking, to the mode prresentation of the VLF propagation in the WGEI, and the other one - to the leakege of VLF beams from the WGEI into

Ann. Geophys. Discuss., https://doi.org/10.5194/angeo-2019-46
Manuscript under review for journal Ann. Geophys.
Discussion started: 7 May 2019

upper ionosphere and magnetosphere and the propagetion in theese media. But we should mention in the present paper only one result which concerns the mode excitation in the WGEI, because this result is principally important for the justification of TIMEB method. Namely, it is shown that the ≥5 lowest modes of the WGEI are strongly localized in the atmosphere-lower ionosphere. Their longitudinal wavenumbers are close to the corresponding wavenumbers of EM waves in the atmosphere. This fact convinces that the TIMEB method can be applied to the propagation of VLF electromagnetic waves in the WGEI.

4. The Results of Modeling

The dependencies of the components of the permittivity ε_1, ε_3, ε_h in the coordinate frame associated with the geomagnetic field $\vec{H}_0$ are given in Fig. 3_2. The typical results of simulations are presented in Fig. 4_3. The parameters of the ionosphere correspond to Fig. 3_2. The inclination of the geomagnetic field is 45°. The VLF frequency is $\omega = 10^5$ s^{-1}, $f = \omega/2\pi \approx 15.9$ kHz. The Earth's surface is assumed as ideally conductive here: $Z = 0$. The values of EM field are given in absolute units, i.e. the magnetic field is measured in Oersteds (Oe), or Gauss (Gs), 1 Gs = 10^{-4} T, whereas the electric field is also in Gs, 1 Gs = 300 V/cm there.

Note that in the absolute (Gaussian) units the magnitudes of the magnetic field component $|H_y|$ are the same as ones of the electric field component $|E_z|$ in the atmosphere region where the permittivity is $\varepsilon \approx 1$. Below in the figure captions the correspondence between the absolute units and practical SI ones is given.

It is seen that the absolute values of the components of the permittivity increase sharply just above $z = 75$ km. The behavior of the components of the permittivity is step-like, as seen from Fig. 3_2, a. Due to this, the results of simulations are tolerant to the choice of the position of the upper wall of the waveguide the Earth's surface – ionosphere. The computed components of the tensor impedance at $z = 85$ km are: $Z_{11} = 0.087 + i0.097$, $Z_{21} = 0.085 + i0.063$, $Z_{12} = -0.083 - i0.094$, $Z_{22} = 0.093 + i0.98$. So, a condition $|Z_{\alpha\beta}| \leq 0.15$ is satisfied there, which is necessary for applicability of the boundary conditions (3).

The maximum value of the H_y component is 0.1 Oe = 10^{-5} T in Fig. 3, a) for the initial VLF beam at $x = 0$. This corresponds to the value of E_z component of 0.1 Gs = 30 V/cm. At the distance $x = 1000$ km the magnitudes of the magnetic field H_y are of about $3 \cdot 10^{-5}$ Oe = 3 nT, whereas ones of the electric field E_y are of about $3 \cdot 10^{-6}$ Gs ≈ 1 mV/cm.

Ann. Geophys. Discuss., https://doi.org/10.5194/angeo-2019-46
Manuscript under review for journal Ann. Geophys.
Discussion started: 7 May 2019

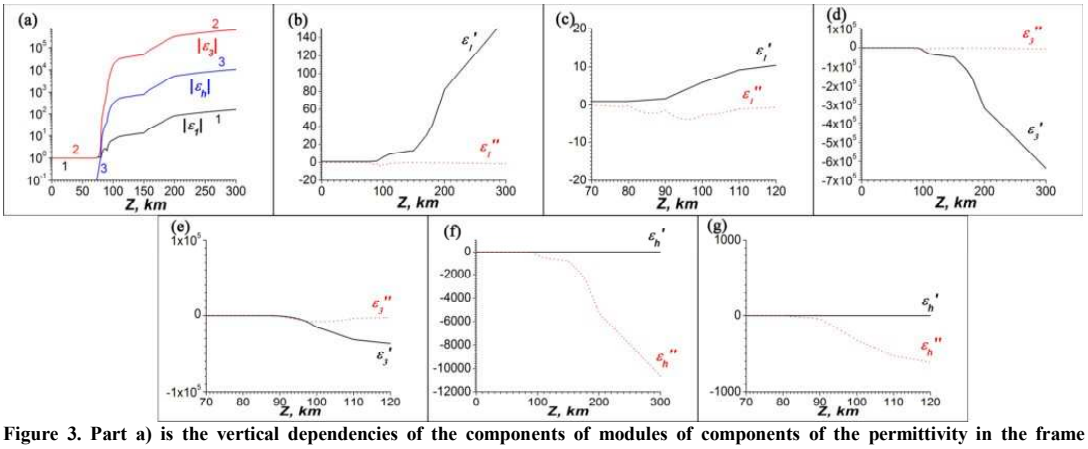

Figure 3. Part a) is the vertical dependencies of the components of modules of components of the permittivity in the frame associated with the geomagnetic field $|\varepsilon_1|$, $|\varepsilon_3|$, $|\varepsilon_h|$, the curves 1, 2, 3 correspondingly. Parts b) – g) are the real and imaginary parts of the components ε_1, ε_3, ε_h, general and detailed views.

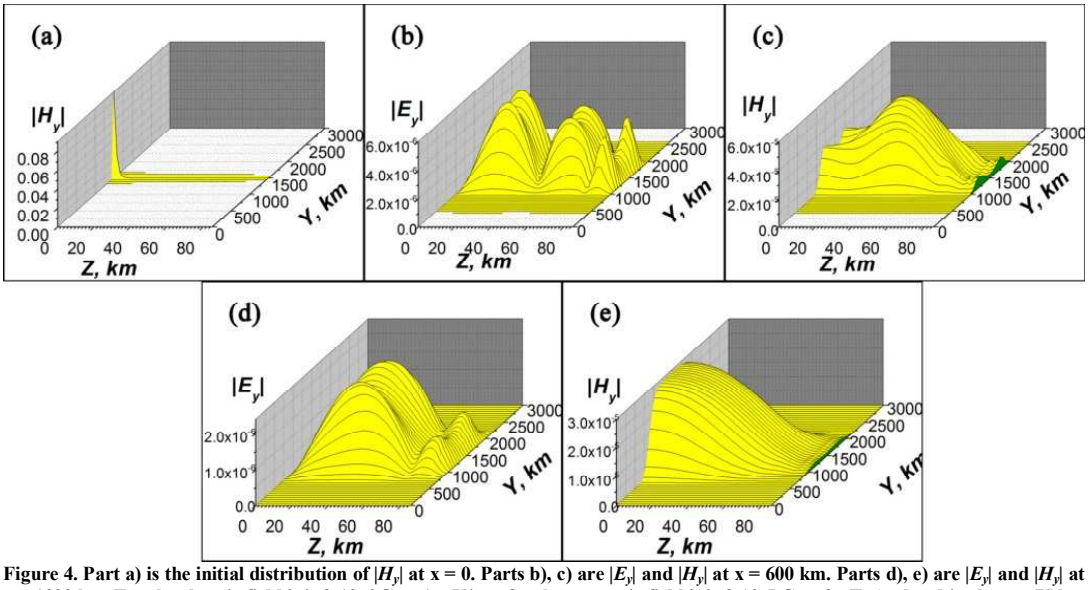

Figure 4. Part a) is the initial distribution of $|H_y|$ at x = 0. Parts b), c) are $|E_y|$ and $|H_y|$ at x = 600 km. Parts d), e) are $|E_y|$ and $|H_y|$ at x = 1000 km. For the electric field it is 3·10-6 Gs ≈ 1 mV/cm, for the magnetic field it is 3·10-5 Gs ≈ 3 nT. At the altitudes z < 75 km it is $|E_z| \approx |H_y|$, so $3 \cdot 10^{-5}$ Gs ≈ 10 mV/cm there.

It is seen from Fig. 4, b) - e), that the wave beams are localized within the waveguide the Earth's surface – ionosphere $0 < z < 75$ km mainly in the regions with the isotropic permittivity. The mutual transformations of the beams of different

Ann. Geophys. Discuss., https://doi.org/10.5194/angeo-2019-46
Manuscript under review for journal Ann. Geophys.
Discussion started: 7 May 2019

polarizations occur near the upper boundary, due to the anisotropy of the ionosphere within the thin layer 75 km < z < 85 km, Fig. 4, b), d). These transformations depend on the values of the components of the permittivity of the ionosphere at the altitudes z > 80 km and the components of the tensor impedance, so the measurements of the phase and amplitude modulations of different EM components near the Earth's surface can yield the information on the properties of the lower and even middle ionosphere.

The qualitative effect is changing the polarization, i.e. an occurrence of E_y component of the electric field at small altitudes z ~ 5 – 10 km near the Earth's surface, due to these mutual transformations of EM beams, Fig. 4, parts b), de). Note that the case of the ideal conductivity of the Earth's surface is considered here, Z = 0, so at z = 0 the component is E_y = 0. If this impedance is $Z \neq 0$, then E_y component occurs also at the Earth's surface.

The magnitudes of E_y component depend essentially on the values of the electron concentration at the altitudes z = 75 - 100 km. In Fig. 5, parts a), b), there are different dependencies of the electron concentration $n(z)$, three curves, solid (1), dash (2), and dot (3) ones. The corresponding dependencies of the absolute values of the components of the permittivity are in Fig. 4, parts c), d).

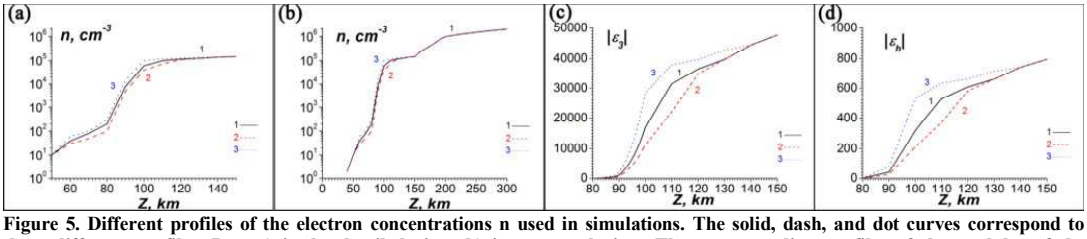

Figure 5. Different profiles of the electron concentrations n used in simulations. The solid, dash, and dot curves correspond to these different profiles. Part a) is the detailed view, b) is a general view. The corresponding profiles of the modules of the components of the permittivity $|\varepsilon_3|$ and $|\varepsilon_h|$ are given in parts c), d).

The distributions of $|E_y|$, $|H_y|$ on z, y at x = 1000 km are given in Fig. 6. Parts a), b) correspond to the solid (1) curve $n(z)$ in Fig. 5; parts c), d) are for the dash (2) curve; parts e), f) are for the dot (3) curve in Fig. 5. The initial beams of H_y are the same and are given in Fig. 4, a). The values of the tensor impedance for these 3 cases are presented in Table 1

Table 1. The values of the tensor impedance corresponding to the data shown in Fig. 5. Impedances presented in the lines 1,2 and 3 in Table one correspond to the solid (1), dash (2) and dot (3) curves in Figs. 5 a)-d), respectively.

Z_{11}	Z_{21}	Z_{12}	Z_{22}
0.088 + i0.098	0.085 + i0.063	-0.083- i0.094	0.093 + i0.098
0.114+i0.127	0.107+i0.079	-0.105-i0.127	0.125+i0.125
0.067+i0.0715	0.061+i0.051	-0.060-i0.070	0.069+i0.072

Ann. Geophys. Discuss., https://doi.org/10.5194/angeo-2019-46
Manuscript under review for journal Ann. Geophys.
Discussion started: 7 May 2019

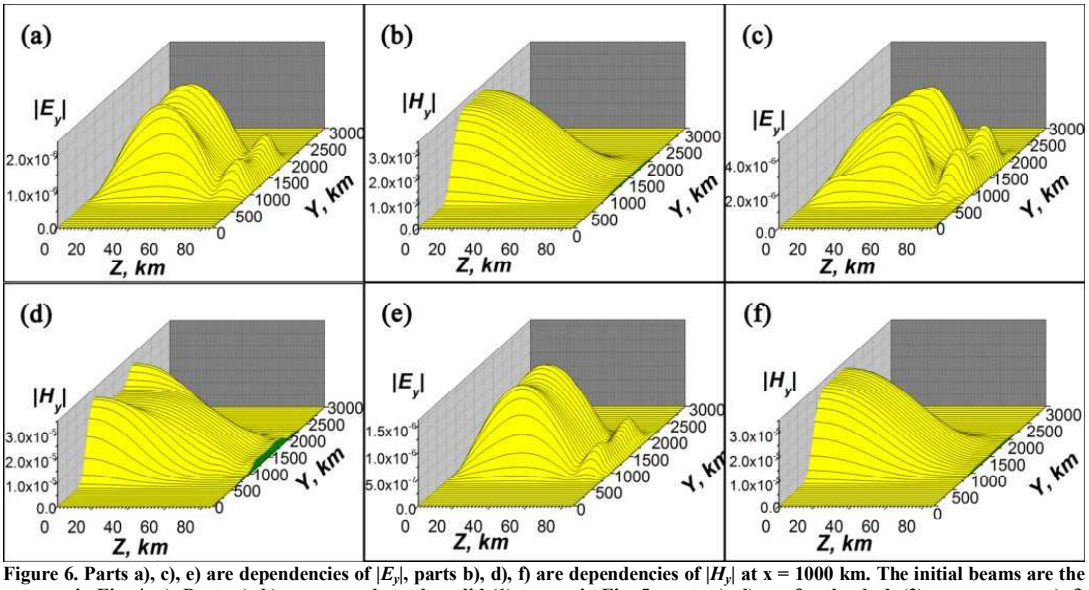

Figure 6. Parts a), c), e) are dependencies of $|E_y|$, parts b), d), f) are dependencies of $|H_y|$ at x = 1000 km. The initial beams are the same as in Fig. 4, a). Parts a), b) corresponds to the solid (1) curves in Fig. 5; parts c), d) are for the dash (2) curves; parts e), f) correspond to the dot (3) curves there. For the electric field it is 3·10-6 Gs ≈ 1 mV/cm, for the magnetic field it is 3·10-5 Gs ≈ 3 nT. At the altitudes z < 75 km it is $|E_z| \approx |H_y|$, so 3·10-5 Gs ≈ 10 mV/cm there.

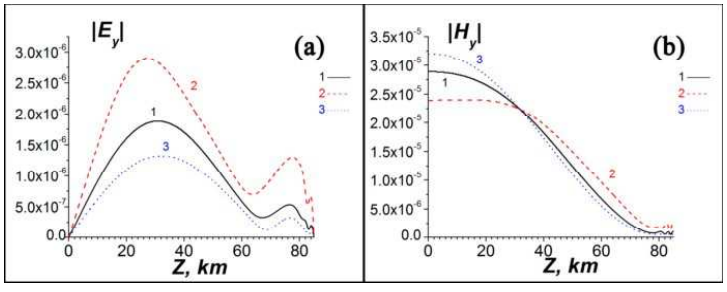

Figure 7. The dependencies of EM components on the altitude z in the center of the waveguide y = 1500 km for the different profiles of the electron concentration. The solid (1), dash (2), and dot (3) curves correspond to the different profiles of the electron concentration in Fig. 5, a), b), the same kinds of curves. For the electric field it is 3·10-6 Gs ≈ 1 mV/cm, for the magnetic field it is 3·10-5 Gs ≈ 3 nT. At the altitudes z < 75 km it is $|E_z| \approx |H_y|$, so 3·10-5 Gs ≈ 10 mV/cm there.

The distributions of $|E_y|$, $|H_y|$ on z at x = 1000 km in the center of the waveguide y = 1500 km are given in Fig. 7. This and other (not presented here) simulations show that change in complex tensors of both volume dielectric permittivity and impedances at the lower and upper boundaries of effective WGEI influence remarkably on the VLF losses in the WGEI. The modulation of the electron concentration at the altitudes above z= 120 km affects weakly the excitation of E_y component within the waveguide.

Ann. Geophys. Discuss., https://doi.org/10.5194/angeo-2019-46
Manuscript under review for journal Ann. Geophys.
Discussion started: 7 May 2019

Annales Geophysicae Discussions
Open Access
EGU

5. Discussion

The observations presented in (Roznoi et al. 2015) demonstrated a possibility for seismogenic increasing losses of VLF waves in the WGEI (Fig. 8; see the details in (Roznoi et al. 2015)). We will discuss the correspondence to these experimental results qualitatively.

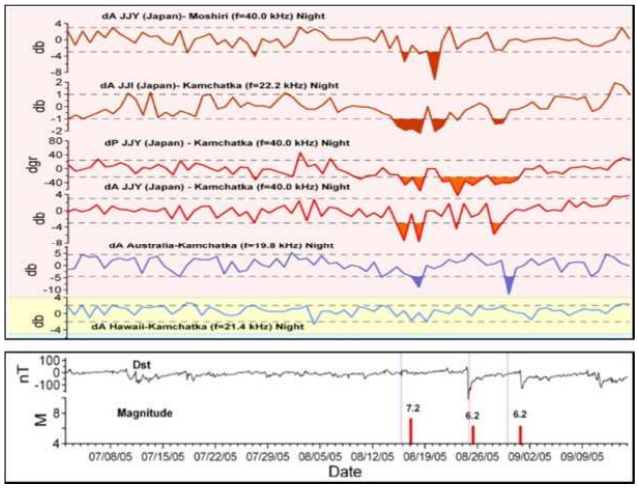

Figure 8. Averaged through night residual VLF/LF signals in the ground observation for the wave paths: JJY-Moshiri, JJI-Kamchatka, JJY-Kamchatka, NWC-Kamchatka, and NPM-Kamchatka. Horizontal dotted lines show the 2σ level. The color filled zones highlight values exceeding the -2σ level. Two panels below are Dst variations and earthquakes magnitude values (from Rozhnoi et al., 2015, but not including the DEMETER data). See other details in (Rozhnoi et al. 2015).

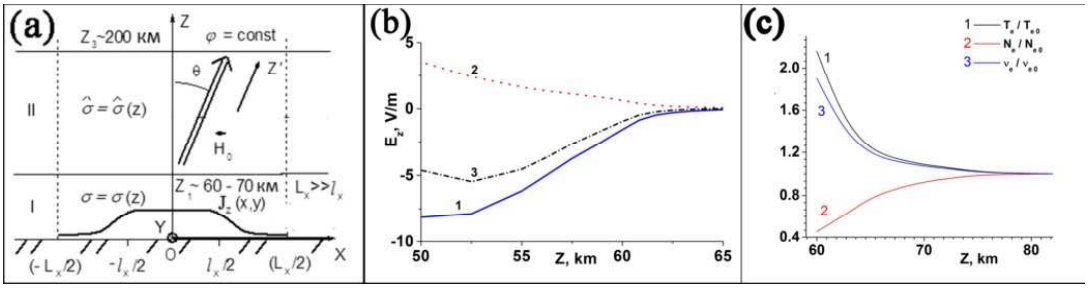

Figure 9. Modification of the ionosphere by electric field of seismogenic origin. (a) – Geometry of the electrostatic problem on the penetration into the ionosphere of the electric field excited by near-ground seismogenic current source; I and II - isotropic and anisotropic regions of the system "atmosphere-ionosphere". (b) Electric field in the mesosphere; in the presence of the current sources in the mesosphere (curve 1), seismogenic current source in the lower atmosphere (curve 2) and both in the mesosphere and in the lower atmosphere (curve 3); current sources in the mesosphere and lower atmosphere are of the same sign and coincide by the sign with fair weather current (directed vertically downward). (c) Relative perturbations (normalized on the

Ann. Geophys. Discuss., https://doi.org/10.5194/angeo-2019-46
Manuscript under review for journal Ann. Geophys.
Discussion started: 7 May 2019

corresponding steady-state values in the absence of perturbing electric field, denoted by the index "0") of electron temperature (T_e / T_{e0}), electron concentration (N_e / N_{e0}), and electron collision frequency (ν_e / ν_{e0}).

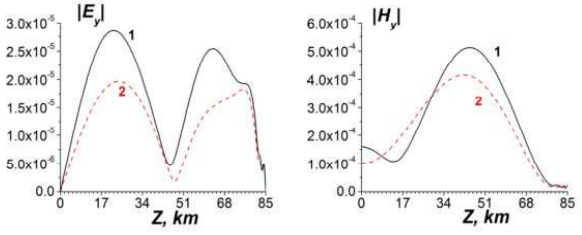

a **b**

Figure 10. Altitude distributions of the normalized tangential (*y*) electric (a) and magnetic (b) VLF beam field components in the central plane of the transverse beam distribution (*y=0*) at the distance *z*=1000 km from the input of the system. Curves 1 in Fig. a, b correspond qualitatively to the presence of only mesospheric electric current source (with relatively smaller value of N_e and larger ν_e) and curves 2 – to the presence of both mesospheric and near-ground seismogenic electric current sources (with relatively larger value of N_e and smaller ν_e); curves 1 and 2 correspond to the identical input beams at *z*=0 (not shown here). Curves 1 and 2 in Fig. 10 a, b correspond qualitatively to the curves 1 and 3 in Fig. 9 b, respectively (see also Fig. 9 c and the caption to that figure).

To do this, account for the modification of the ionosphere due to electric field excited by the near-ground seismogenic current source. In the model (Rapoport et al. 2006), the presence of the mesospheric current source, which reflects the observations (Martynenko 2004; Meek 2001; Bragin 1974) is taken into account, and curve 1 in Fig. 9 b the corresponding vertical field distribution in the mesosphere. It is supposed that the mesospheric current has only *Z* component and is positive, what means that it is directed vertically downward, as well as fair-weather current (curve 1, Fig. 8). Then suppose that near-ground seismogenic current is directed in the same way, as mesospheric current. If the mesospheric current is equal to zero and only corresponding seismogenic near-ground current is present. Corresponding mesospheric electric field, under the condition of given difference of the potentials between the Earth and the ionosphere (curve 2, Fig. 9 b), is directed oppositely to those excited by the corresponding mesospheric current (curve 1, Fig. 9 b). As a result, in the presence of both mesospheric and seismogenic near-ground current, the total mesospheric electric field (curve 3, Fig. 8 b) is less by the absolute value, than those in the presence of *only* mesospheric current (curve 1, Fig. 9 b). As it is shown in (Rapoport et al. 2006), the decrement of losses $|k''|$ for VLF waves in the WGEI is proportional to $|k''| \sim |\varepsilon''| \sim N_e / \nu_e$. Accounting for that in the external electric field in the mesosphere N_e and ν_e decreases and increases, respectively, due to the appearance of seismogenic near-ground electric current, in addition to the mesospheric current (curve 3, Fig. 9 b), losses increases comparatively to the case, when the seismogenic current is absent and electric field is larger by absolute value (curve 1, Fig. 9 b). An increasing in VLF beam losses, shown in Fig 10 corresponds to increasing losses with increasing absolute value of imaginary part of the dielectric permittivity when near-ground seismogenic current source (curves 2 in Fig. 9 a, b) appear, additionally to the pre-existing mesospheric current source (curves 1 in Fig. 9 a, b, see also caption to the Fig. 9). This corresponds qualitatively to the results presented in (Roznoi et al. 2015), see also Figs. 8. Note that the above mentioned

estimations concern only volume losses in the WGEI. Losses connected with the modification of effective impedance are not included in the course of these elementary estimations, and the more detailed consideration of both the modification of the ionosphere by means of electric-photochemistry mechanism and the variation of losses due to all mechanisms including volume and effective impedance effects will be a subject of the subsequent papers.

The closest approach to a direct investigation of the profile of VLF electromagnetic field in the Earth-Ionosphere waveguide was a series of sounding rocket campaigns at mid- and high-latitudes [Wallops Is., VA, and Siple Station, Antarctica - Kintner et al.,1983; Brittain et al., 1983; Siefring and Kelly, 1991; Arnoldy and Kintner, 1989] where single-axis E-field and three-axis B-field antennas, supplemented in some cases with in situ plasma density measurements were used to detect the far-field fixed-frequency VLF signals radiated by US Navy and Stanford ground transmitters.

The most comprehensive study of the WGEI will be provided by the ongoing NASA VIPER (VLF Trans-Ionospheric Propagation Experiment Rocket) project (PI J. W. Bonnell, UC Berkeley, NASA Grant 80NSSC18K0782). The VIPER sounding rocket campaign is consist of a summer nighttime launch during quiet magnetosphere conditions from Wallops Flight Facility, VA, collecting data through the D, E, and F regions of the ionosphere with a payload carrying the following instrumentation: 2D E- and 3D B-field waveforms, DC-1 kHz; 3D ELF to VLF waveforms, 100 Hz to 50 kHz; 1D wideband E-field measurement of plasma and upper hybrid lines, 100 kHz to 4 MHz; and Langmuir probe plasma density and ion gauge neutral density measurements at a sampling rate of at least tens of Hz. The VIPER project will fly a fully 3D EM field measurement, DC through VLF, and relevant plasma and neutral particle measurements at mid-latitudes through the radiation fields of (1) an existing VLF transmitter (the VLF transmitter Cutler with call sign NAA, the very low frequency (VLF) shore radio station at Cutler, Maine, USA, which transmits, at a frequency of 24 kHz an input power of up to 1.8 megawatts, see Fig. 11) and (2) naturally-occurring lightning transients through and above the leaky upper boundary of the WGEI supported by a vigorous theory and modelling effort in order to explore the vertical and horizontal profile of the observed 3D electric and magnetic radiated fields of the VLF transmitter, and the profile related to the observed plasma and neutral densities. The VLF waves reflection, absorption, and transmission processes as a function of altitude will be searched making use of the data on the vertical VLF E- and B-field profile

Ann. Geophys. Discuss., https://doi.org/10.5194/angeo-2019-46
Manuscript under review for journal Ann. Geophys.
Discussion started: 7 May 2019

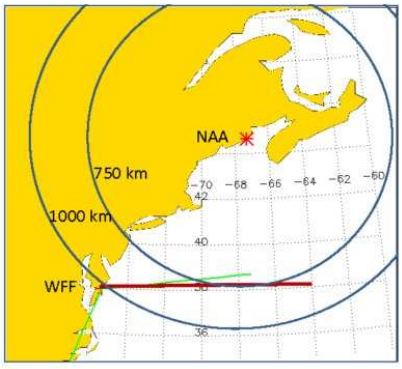

Figure 11. Proposed VIPER Trajectory

The aim of this experiment is the investigation of the VLF beams launched by the near-ground source/VLF transmitter with the known parameters and propagating both in the WGEI and leaking from WGEI into the upper ionosphere. Characteristics of these beams will be compared with the theory proposed in the present paper and the theory on leakage of the VLF beams from WGEI, which we will present in the next papers.

Conclusions

(1) We have devoloped the new and highly effective robust method of tensor impedance for the VLF electromagnetic beam propagation in the inhomogeneous waveguiding media - "tensor impedance method for modelling propagation of electromagnetic beams (TIMEB)" in a multi-layered/inhomogeneous waveguide.

(2) The main differences/advantages of the proposed tensor impedance method in comparison with the known method of the impedance recalculating, in particular invariant imbedding methods (Shalashov and Gospodchikov, 2010; Kim and Kim, 2016) are the following: (i) our method is a direct method of the recalculation of tensor impedance, and the corresponding tensor impedance is determined analytically, see Eqs. (22). (ii) Our method, for the media without non-locality, does not needs a solution of integral equation(s), as the invariant imbedding method does (iii) The proposed tensor impedance method does not need the revealing of forward and reflected waves. Moreover, even the conditions of the radiation (12) at the upper boundary $z=L_{max}$ is determined through the total field components $H_{x,y}$, what makes the proposed procedure technically less cumbersome and practically more convenient.

(3) The application of this method jointly with the previous results of the modification of the ionosphere by seismogenic electric field gives the results, which qualitatively are in an agreement with the experimental data on the seismogenic increasing losses of VLF waves/beams propagating in the WGEI.

(4) The waveguide includes the region for the altitudes $0 < z < 80$ - 90 km. The boundary conditions are the radiation conditions at z = 300 km, they can be recalculated to the lower altitudes as the tensor relations between the tangential components of the EM field. In another words, the tensor impedance conditions have been used at z = 80 – 90 km.

(5) The observable qualitative effect is mutual transformations of different polarizations of the electromagnetic field occur during the propagation. This transformation of the polarizations depends on the electron concentration, i.e. the conductivity, of D- and E-layers of the ionosphere at the altitudes 75 – 120 km.

(6) Change in complex tensors of both volume dielectric permittivity and impedances at the lower and upper boundaries of effective WGEI influence remarkably on the VLF losses in the WGEI.

(7) The proposed model and results on propagation of VLF electromagnetic beams in the WGEI will be useful to explore the characteristics of these waves as an effective instrument for diagnostics the influences on the ionosphere "from above" (Sun-Solar Wind-Magnetosphere-Ionosphere), "from below""(the most powerful meteorological, seismogenic and other sources in the lower atmosphere and lithosphere/Earth, such as hurricanes, earthquakes, tsunamis etc.), from inside the ionosphere (strong thunderstorms and lightning discharges) and even from the far space (such as gamma-flashes, cosmic rays etc.).

ACKNOWLEDGMENTS

The work of OA and JB was supported by the NASA Grant 80NSSC18K0782. V.F. thanks the NERC for financial support

REFERENCES

Agapitov, O. V., Artemyev, A. V., Mourenas, D., Kasahara, Y., and Krasnoselskikh, V.: Inner belt and slot region electron lifetimes and energization rates based on AKEBONO statistics of whistler waves, J. Geophys. Res.: Space Phys., 119, 2876–2893, https://doi.org/10.1002/2014JA019886, 2014.

Agapitov, O. V., Mourenas, D., Artemyev, A. V., Mozer, F. S., Hospodarsky, G., Bonnell, J., and Krasnoselskikh, V: Synthetic Empirical Chorus Wave Model From Combined Van Allen Probes and Cluster Statistics, J. Geophys. Res.: Space Phys., 123, 2017JA024843, https://doi.org/10.1002/2017JA024843, 2018.

Alperovich, L. S. and Fedorov, E. N.: Hydromagnetic Waves in the Magnetosphere and the Ionosphere, Springer, 426 pp., 2007.

Arnoldy, R. L. and Kintner, P. M.: Rocket observations of the precipitation of electrons by ground VLF transmitters, J. Geophys. Res.: Space Phys., 94, 6825–6832, https://doi.org/10.1029/JA094iA06p06825, 1989.

Artsimovich, L. A. and Sagdeev, R. Z: Physics of plasma for physicists, ATOMIZDAT Publ. House, Moscow, 320 pp., 1979 (in Russian).

Artemyev, A. V., Agapitov, O. V., Mourenas, D., Krasnoselskikh, V., and Zelenyi, L. M.: Storm-induced energization of radiation belt electrons: Effect of wave obliquity, Geophys. Res. Lett., 40, 4138–4143, https://doi.org/10.1002/grl.50837, 2013.

Artemyev, A., Agapitov, O., Mourenas, D., Krasnoselskikh, V., and Mozer, F.: Wave energy budget analysis in the Earth's radiation belts uncovers a missing energy, Nat. Commun., 6, https://doi.org/10.1038/ncomms8143, 2015.

Azadifar, M., Li, D., Rachidi, F., Rubinstein, M., Diendorfer, G., Schulz, W., Pichler, H., Rakov, V. A., Paolone, M., Pavanello, D.: Analysis of lightning-ionosphere interaction using simultaneous records of source current and 380-km distant electric field, Journ. Atmos. Solar-Terrestr. Phys., 159, 48–56, https://doi.org/10.1016/j.jastp.2017.05.010, 2017.

Beletskii, N. N., Borysenko, S. A., and Gvozdev, N. I.: The Resonant Interaction of Electromagnetic Waves in a Defect Dielectric Periodic Layered Structure Placed in a Parallel-Plate Waveguide, Radiophys. Electron., 5, 7 pp., https://doi.org/10.1615/TelecomRadEng.v75.i6.40, 2014.

Biagi, P. F., Maggipinto, T., and Ermini, A.: The European VLF/LF radio network: current status, Acta Geod. Geophys., 50, 109–120, https://doi.org/10.1007/s40328-014-0089-x, 2015.

Biagi, P. F., Maggipinto, T., Righetti, F., Loiacono, D., Schiavulli, L., Ligonzo, T., Ermini, A., Moldovan, I. A., Moldovan, A. S., Buyuksarac, A., Silva, H. G., Bezzeghoud ,M., and Contadakis, M. E.: The European VLF/LF radio network to search for earthquake precursors: setting up and natural/man-made disturbances, Nat. Hazards Earth Syst. Sci., 11, 333–341, https://doi.org/10.5194/nhess-11-333-2011, 2011.

Boudjada, M. Y., Schwingenschuh, K., Al-Haddad, E., Parrot, M., Galopeau, P. H. M., Besser, B., Stangl, G., and Voller, W., Effects of solar and geomagnetic activities on the sub-ionospheric very low frequency transmitter signals received by the DEMETER micro-satellite, Ann. Geo., 55, 1, https://doi.org/10.4401/ag-5463, 2012.

Bragin, Yu. A., Tyutin Alexander, A., Kocheev, A.A., and Tyutin, Alexei, A.: Direct measurements of the vertical electric field of the atmosphere up to 80 km, Space Res., 12, 279–281, 1974.

Brittain, R., Kintner, P. M., Kelley, M. C., Siren, J. C., and Carpenter, D. L.: Standing wave patterns in VLF Hiss, J. Geophys. Res.: Space Phys., 88, 7059–7064, https://doi.org/10.1029/JA088iA09p07059, 1983.

Buitink, S., Corstanje, A., Enriquez, J. E., Falcke, H., Hörandel ,J. R., Huege, T., Nelles, A., Rachen, J. P., Schellart, P., Scholten, O., ter Veen, S., Thoudam, S., and Trinh, T. N. G.: A method for high precision reconstruction of air shower X_{max} using two-dimensional radio intensity profiles, arXiv:1408.7001v2 [astro-ph.IM], 1 Sep 2014.

Chevalier, M. W., Inan U. S.: A Technique for Efficiently Modeling Long-Path Propagation for Use in Both FDFD and FDTD, IEEE Ant. Wireless Propag. Lett., 5, 525-528, https://doi.org/10.1109/LAWP.2006.887551, 2006

Chou, M.-Y., Lin, C. C. H., Yue, J., Chang, L. C., Tsai, H.-F., and Chen, C.-H., Medium-scale traveling ionospheric disturbances triggered by Super Typhoon Nepartak, Geophys. Res. Lett., 44, 7569–7577, https://doi.org/10.1002/2017gl073961, 2017.

Collin, R. E., *Foundations for Microwave Engineering*. New York: John Willey & Sons, Inc., 2001.

Cummer, S. A., Inan ,U. S., Bell, T. F., and Barrington-Leigh, C. P.: ELF radiation produced by electrical currents in sprites, Geophys. Res. Lett., 25, 1281–1284, https://doi.org/10.1029/98GL50937, 1998.

Cummer, S. A., Briggs, M. S., Dwyer, J. R., Xiong, S., Connaughton, V., Fishman, G. J., Lu, G., Lyu, F., and Solanki, R.: The source altitude, electric current, and intrinsic brightness of terrestrial gamma ray flashes, Geophys. Res. Lett., 41, https://doi.org/10.1002/2014GL062196, 2014.

Dwyer, J. R. and Uman, M. A.: The physics of lightning, Phys. Rep., 534, 147–241, https://doi.org/10.1016/j.physrep.2013.09.004, 2014.

Dwyer, J. R.: The relativistic feedback discharge model of terrestrial gamma ray flashes, Journ. Geophys. Res., 117, A02308, https://doi.org/10.1029/2011JA017160, 2012

Grimalsky, V.V., Kremenetsky, I.A., Rapoport, Yu.G.: Excitation of electromagnetic waves in the lithosphere and their penetration into ionosphere and magnetosphere, J. of Atmosph. Electricity,19, 101-117, 1999 a.

Grimalsky, V.V., Kremenetsky, I.A., Rapoport, Yu.G.: Excitation of EMW in the lithosphere and propagation into magnetosphere . In: "Atmospheric and Ionospheric Electromagnetic Phenomena Associated with Earthquakes". Ed.: M. Hayakawa. (TERRAPUB), Tokyo, 777-787, 1999 b.

Gurevich, A V, Zybin, K P.: Runaway breakdown and electric discharges in thunderstorms, Physics – Uspekhi, 44, 11, 1119 – 1140, https://doi.org/10.1070/PU2001v044n11ABEH000939, 2001

Gurevich, A V., Karashtin, A N., Ryabov, V A., Chubenko, A L Shepetov: Nonlinear phenomena in the ionospheric plasma.Effects of cosmic rays and runaway breakdown on thunderstorm discharges, Physics - Uspekhi 52 (7), 735-745, https://doi.org/0.3367/UFNe.0179.200907h.0779, 2009

Hapgood, M.: Space Weather, IOP Publ., Bristol, 23 PP., https://doi.org/10.1088/978-0-7503-1372-8, 2017

Hare, B. M., Scholten, O., Bonardi, A., Buitink, S., Corstanje, A., Ebert, U., Falcke, H., Hörandel, J. R., Leijnse, H., Mitra, P., Mulrey, K., Nelles, A., Rachen, J. P., Rossetto, L., Rutjes, C., Schellart, P., Thoudam, S., Trinh, T. N. G., ter Veen, S., and Winchen, T., LOFAR Lightning Imaging: Mapping Lightning With Nanosecond Precision, J. Geophys. Res.: Atmospheres, 123, 2861–2876, https://doi.org/10.1002/2017JD028132, 2018.

Hayakawa, M.: Earthquake prediction with radio techniques, Wiley, Singapore, 294 P., 2015.

Horne, R. B., Thorne, R. M., Shprits, Y. Y., Meredith, N. P., Glauert, S. A., Smith, A. J., Kanekal, S. G.,Baker, D. N., Engebretson, M. J., Posch, J. L., Spasojevic, M., Inan, U. S., Pickett, J. S., and Decreau, P. M. E.: Wave acceleration of electrons in the Van Allen radiation belts. Nature, 437, 227–230, https://doi.org/10.1038/nature03939, 2005

Kim, S. and Kim, K.: Invariant imbedding theory of wave propagation in arbitrarily inhomogeneous stratified bi-isotropic media, J. Opt. 18, 065605 (9pp), https://doi.org/10.1088/2040-8978/18/6/065605, 2016.

Kintner, P. M., Brittain, R., Kelley, M. C., Carpenter, D. L., and Rycroft, M. J., In situ measurements of transionospheric VLF wave injection, J. Geophys. Res.: Space Phys., 88, 7065–7073, https://doi.org/10.1029/JA088iA09p07065, 1983.

Kong, J. A., Electromagnetic Wave Theory, New York: John Willey & Sons, Inc., 1990.

Koskinen, H. E. J., Physics of Space Storms. From the Solar Surface to the Earth, Springer-Verlag, 419 P., 2011.

Kurushin, E. P. and Nefedov E. I.: Electrodynamics of anisotropic waveguiding structures, Moscow: Nauka (Science), 1983 (in Russian).

Kuzichev, I.V., Shklyar, D.R.: On full-wave solution for VLF waves in the near-Earth space, Journ. Atmos. Solar-Terrestr. Phys., 72 , 1044–1056, https://doi.org/10.1016/j.jastp.2018.07.002, 2010

Kuzichev, I.V., Vasko, I. Yu., Malykhin, A. Yu., Soto-Chavez, A. R.: On the ionospheric propagation of VLF waves generated by currents in the lower ionosphere, Journ. Atmos. Solar-Terrestr. Phys., 179, 138-148, https://doi.org/10.1016/j.jastp.2018.07.002, 2010

Lehtinen, N. G., Inan U. S.: Radiation of ELF/VLF waves by harmonically varying currents into a stratified ionosphere with application to radiation by a modulated electrojet, Journ Geophys. Res., 113, A06301, https://doi.org/10.1029/2007JA012911, 2008

Lehtinen, N. G., Inan U. S.: Full-wave modeling of transionospheric propagation of VLF waves, Geophys. Res. Lett., 36, L03104, https://doi.org/10.1029/2008GL036535, 2009

Levy, M.: Parabolic equation methods for electromagnetic wave propagation, The Inst. of Electrical Eng., Padstow, Cornwall, 336 P., 2000

Lu, G., Zhang, H., Cummer, S. A., Wang, Y., Lyu, F., Briggs, M., Xiong, S., Chen, A.: A comparative study on the lightning sferics associated with terrestrial gamma-ray flashes observed in Americas and Asia, Journ. Atmos. Solar-Terrestr. Phys. 183, 67–75, https://doi.org/10.1016/j.jastp.2019.01.001, 2019

Maier, S. A.: Plasmonics: Fundamentals and Applications, N. Y.: Springer, 234 p., 2007.

Marshall, R. A., Wallace, T.: Finite-Difference Modeling of Very-Low-Frequency Propagation in the Earth-Ionosphere Waveguide, IEEE Trans. Ant. Propag., 65, 7185-7197, https://doi.org/10.1109/TAP.2017.2758392, 2017

Martynenko, S. I., Rozumenko, V. T., and Tyrnov, O. F.: New possibilities for mesospheric electricity diagnostics, Adv. Space Res., 27, 1127–1132, https://doi.org/10.1016/S0273-1177(01)00208-3, 2001.

Meek, C. E., Manson, A. H., Martynenko, S. I., Rozumenko, V. T., and Tyrnov, O. F.: Remote sensing of mesospheric electric fields using MF radars, J. Atmos. Sol.-Terr. Phys., 66, 881–890, https://doi.org/10.1016/j.jastp.2004.02.002, 2004.

Mezentsev, A., Lehtinen, N., Ostgaard, N., Perez-Invernon, F. J., and Cummer, S. A.: Spectral characteristics of VLF sferics associated with RHESSI TGFs, J. Geophys. Res.: Atmospheres, 123, https://doi.org/10.1002/2017JD027624, 2018.

Nina, A., Radovanović, M., Milovanović, B., Kovačević, A., Bajčetić, J., and Popović, L. C.: Low ionospheric reactions on tropical depressions prior hurricanes, Adv. Space Res., 60, 1866–1877, https://doi.org/10.1016/j.asr.2017.05.024, 2017.

Qin, J., Celestin, S., and Pasko, V. P.: Low frequency electromagnetic radiation from sprite streamers, Geophys. Res. Lett., 39, L22803, https://doi.org/10.1029/2012GL053991, 2012.

Patra, S., Spencer, E. Horton, W. and Sojka, J.: Study of Dst/ring current recovery times using the WINDMI model, Journ. Geophys. Res., 116, A02212, https://doi.org/10.1029/2010JA015824, 2011

Rapoport, Yu. G., Boardman, A. D., Grimalsky, V. V., Ivchenko, V. M., Kalinich, N: Strong nonlinear focusing of light in nonlinearly controlled electromagnetic active metamaterial field concentrators, J. Opt. (United Kingdom), 16, 0552029–0552038, https://doi.org/10.1088/2040-8978/16/5/055202, 2014.

Rapoport, Yu. G., Gotynyan, O. E., Ivchenko, V. N., Hayakawa, M., Grimalsky, V. V., Koshevaya, S. V., Juarez, D.: Modeling electrostatic – photochemistry seismoionospheric coupling in the presence of external currents, Phys. Chem. Earth, 31, 4-9, 437–446, https://doi.org/10.1016/j.pce.2006.02.010, 2006

Richmond, A. D.: Space Weather Research Prompts Study of Ionosphere and Upper Atmospheric Electrodynamics, EOS, Trans. , Amer. Geophys. Union, 77,(11), 101, https://doi.org/10.1029/96eo00066, 1996

Rozhnoi, A., Solovieva, M., Levin, B., Hayakawa, M., and Fedun, V.: Meteorological effects in the lower ionosphere as based on VLF/LF signal observations, Nat. Hazards Earth Syst. Sci., 14, 2671–2679, https://doi.org/10.5194/nhess-14-2671-2014, 2014.

Rozhnoi, A., Solovieva, M., Parrot, M., Hayakawa, M., Biagi, P.-F., Schwingenschuh, K., Fedun, V.: VLF/LF signal studies of the ionospheric response to strong seismic activity in the Far Eastern region combining the DEMETER and ground-based observations, Phys. Chem. Earth, 85–86, 141–149, https://doi.org/10.1016/j.pce.2015.02.005, 2015.

Ruibys G. and Tolutis R.: Nonreciprocal HF signal transmission by surface helicon. Electronics Letters, 19(8), 273. https://doi.org/10.1049/el:19830191, 1983

Samarskii, A.A.: The Theory of Difference Schemes, Marcel Dekker, N.Y., 2001.

Sanchez-Dulcet, F., Rodriguez-Bouza M., Silva, H. G., Herraiz, M., Bezzeghoud, M., Biagi, P. F.: Analysis of observations backing up the existence of VLF and ionospheric TEC anomalies before the Mw6.1 earthquake in Greece, January 26, 2014, Phys. Chem. Earth, 85–86, 150–166, https://doi.org/10.1016/j.pce.2015.07.002, 2015.

Scholten, O., Bonardi, A., Buitink, S., Corstanje, A., Ebert, U., Falcke, H., Hörandel, J., Mitra, P., Mulrey, K., Nelles, A., Rachen, J., Rossetto, L., Rutjes, C., Schellart, P., Thoudam, S., Trinh, G., ter Veen, S., and Winchen, T. Precision study of radio emission from air showers at LOFAR, EPJ Web of Conferences, 136, 02012, https://doi.org/10.1051/epjconf/201713602012, 2017.

Senior, T. B. A. and J. L. Volakis: Approximate boundary conditions in electromagnetics, London: Institution of Electrical Engineers, 1995.

Shalashov, A. G. and Gospodchikov, E. D.: Impedance technique for modeling electromagnetic wave propagation in anisotropic and gyrotropic media, Physics-Uspekhi, 54, 145–165, https://doi.org/10.3367/UFNe.0181.201102c.0151, 2011.

Siefring, C. L. and Kelley, M. C.: Analysis of standing wave patterns in VLF transmitter signals: Effects of sporadic E layers and in situ measurements of low electron densities, J. Geophys. Res.: Space Phys., 96, 17813–17826, https://doi.org/10.1029/91JA00615, 1991.

Spiegel, M. R.: Theory and problems of vector analysis and an introduction to tensor analysis, Shnaum Publ., NY, 223 P., 1959.

Surkov, V. and Hayakawa, M.: Ultra and Extremely Low Frequency Electromagnetic Fields, Springer, Tokyo, 2014.

Tarkhanyan, R. H. and Uzunoglu, N. K., Radiowaves and Polaritons in Anisotropic Media, Weinheim: Wiley-VCH, 210 p., 2006.

Thorne, R. M.: Radiation belt dynamics: The importance of wave-particle interactions, Geophys. Res. Lett., 372, 22107, https://doi.org/10.1029/2010GL044990, 2010.

Tretyakov, S.: Analytical Modeling in Applied Electromagnetics, Artech House, Boston, 2003.

Walker, A.D. M.: The Theory of Whistler Propagation, Rev. Geophys. Space Phys., 14, 629-638, 1976

Weiland, J. and Wilhelmsson, H.: Coherent Non-Linear Interaction of Waves in Plasmas, Pergamon, London, 1977.

Weit J. R.: Electromagnetic waves in stratified media, New York: IEEE Press and Oxford Univ. Press, 1996.

Wu, C.-C., Liou, K., Lepping, R. P., Hutting, L., Plunkett, S., Howard, R. A., Socker, D.: The first super geomagnetic storm of solar cycle 24: "The St. Patrick's day event (17 March 2015)", Earth, Planets and Space, 68, 151, https://doi.org/10.1186/s40623-016-0525-y, 2016.

Yiğit, E., Koucká Knížová, P., Georgieva, K., & Ward, W.: A review of vertical coupling in the Atmosphere–Ionosphere system: Effects of waves, sudden stratospheric warmings, space weather, and of solar activity, Solar-Terrestrial Physics, 141, 1–12, https://doi.org/10.1016/j.jastp.2016.02.011, 2016

Yu, Ya., Niu, J., Simpson, J. J.: A 3-D Global Earth-Ionosphere FDTD Model Including an Anisotropic Magnetized Plasma Ionosphere, IEEE Trans. Ant. Propag., 3246-3256, https://doi.org/10.1109/TAP.2012.2196937, 2012

Appendix: the matrix coefficients included into eq. (16)

Here the expressions of the matrix coefficients are presented that are used in the matrix factorization to compute the tensor impedance, see eq. (16).

$$\hat{\alpha}_N^{(0)} = \begin{pmatrix} 1+\frac{ih_z}{\Delta}(k_1-\alpha_1\alpha_2 k_2); & \frac{ih_z}{\Delta}\alpha_2(k_2-k_1) \\ \frac{ih_z}{\Delta}\alpha_1(k_1-k_2); & 1+\frac{ih_z}{\Delta}(k_2-\alpha_1\alpha_2 k_1) \end{pmatrix}, \quad \hat{\alpha}_N^{(-)} = \begin{pmatrix} -1; & 0 \\ 0; & -1 \end{pmatrix}; \quad \Delta \equiv 1-\alpha_1\alpha_2;$$

$$\hat{\alpha}_j^{(-)} = \begin{pmatrix} (\frac{\beta_{22}}{1-\beta_{22}\frac{k_x^2}{k_0^2}})_{j-1/2}; & -(\frac{\beta_{21}}{1-\beta_{22}\frac{k_x^2}{k_0^2}})_{j-1/2} + \frac{ik_xh_z}{2}(\frac{\beta_{23}}{1-\beta_{22}\frac{k_x^2}{k_0^2}})_{j-1} \\ -(\frac{\beta_{12}}{1-\beta_{22}\frac{k_x^2}{k_0^2}})_{j-1/2} + \frac{ik_xh_z}{2}(\frac{\beta_{32}}{1-\beta_{22}\frac{k_x^2}{k_0^2}})_{j-1}; & (\beta_{11}+\frac{k_x^2}{k_0^2}\frac{\beta_{12}\cdot\beta_{21}}{1-\beta_{22}\frac{k_x^2}{k_0^2}})_{j-1/2} - \frac{ik_xh_z}{2}(\beta_{13}+\frac{k_x^2}{k_0^2}\frac{\beta_{12}\cdot\beta_{23}}{1-\beta_{22}\frac{k_x^2}{k_0^2}})_{j-1} - \\ & -\frac{ik_xh_z}{2}(\beta_{31}+\frac{k_x^2}{k_0^2}\frac{\beta_{32}\cdot\beta_{21}}{1-\beta_{22}\frac{k_x^2}{k_0^2}})_j \end{pmatrix}$$

Ann. Geophys. Discuss., https://doi.org/10.5194/angeo-2019-46
Manuscript under review for journal Ann. Geophys.
Discussion started: 7 May 2019

Annales Geophysicae Discussions
Open Access
EGU

$$\hat{\alpha}_j^{(+)} = \begin{pmatrix} \left(\frac{\beta_{22}}{1-\beta_{22}\frac{k_x^2}{k_0^2}}\right)_{j+1/2}; & -\left(\frac{\beta_{21}}{1-\beta_{22}\frac{k_x^2}{k_0^2}}\right)_{j+1/2} - \frac{ik_xh_z}{2}\left(\frac{\beta_{23}}{1-\beta_{22}\frac{k_x^2}{k_0^2}}\right)_{j+1} \\ -\left(\frac{\beta_{12}}{1-\beta_{22}\frac{k_x^2}{k_0^2}}\right)_{j+1/2} - \frac{ik_xh_z}{2}\left(\frac{\beta_{32}}{1-\beta_{22}\frac{k_x^2}{k_0^2}}\right)_{j+1}; & \left(\beta_{11} + \frac{k_x^2}{k_0^2}\frac{\beta_{12}\cdot\beta_{21}}{1-\beta_{22}\frac{k_x^2}{k_0^2}}\right)_{j+1/2} + \frac{ik_xh_z}{2}\left(\beta_{13} + \frac{k_x^2}{k_0^2}\frac{\beta_{12}\cdot\beta_{23}}{1-\beta_{22}\frac{k_x^2}{k_0^2}}\right)_{j+1} + \\ & + \frac{ik_xh_z}{2}\left(\beta_{31} + \frac{k_x^2}{k_0^2}\frac{\beta_{32}\cdot\beta_{21}}{1-\beta_{22}\frac{k_x^2}{k_0^2}}\right)_j \end{pmatrix}$$

$$\hat{\alpha}_j^{(0)} = \begin{pmatrix} -\left(\frac{\beta_{22}}{1-\beta_{22}\frac{k_x^2}{k_0^2}}\right)_{j-1/2} - \left(\frac{\beta_{22}}{1-\beta_{22}\frac{k_x^2}{k_0^2}}\right)_{j+1/2} + k_0^2h_z^2; & \left(\frac{\beta_{21}}{1-\beta_{22}\frac{k_x^2}{k_0^2}}\right)_{j-1/2} + \left(\frac{\beta_{21}}{1-\beta_{22}\frac{k_x^2}{k_0^2}}\right)_{j+1/2} \\ \left(\frac{\beta_{12}}{1-\beta_{22}\frac{k_x^2}{k_0^2}}\right)_{j-1/2} + \left(\frac{\beta_{12}}{1-\beta_{22}\frac{k_x^2}{k_0^2}}\right)_{j+1/2}; & -\left(\beta_{11} + \frac{k_x^2}{k_0^2}\frac{\beta_{12}\cdot\beta_{21}}{1-\beta_{22}\frac{k_x^2}{k_0^2}}\right)_{j-1/2} - \left(\beta_{11} + \frac{k_x^2}{k_0^2}\frac{\beta_{12}\cdot\beta_{21}}{1-\beta_{22}\frac{k_x^2}{k_0^2}}\right)_{j+1/2} + \\ & + k_0^2h_z^2\cdot\left(1-\beta_{33}\frac{k_x^2}{k_0^2} - \frac{k_x^4}{k_0^4}\frac{\beta_{23}\cdot\beta_{32}}{1-\beta_{22}\frac{k_x^2}{k_0^2}}\right)_j \end{pmatrix}.$$